Review

Recent Developments in Generation, Detection and Application of Nanobubbles in Flotation

Sabereh Nazari [1], Ahmad Hassanzadeh [2,3,*], Yaqun He [1,*], Hamid Khoshdast [4] and Przemyslaw B. Kowalczuk [2,*]

[1] School of Chemical Engineering and Technology, China University of Mining and Technology, Xuzhou 221116, China; saharnazari2626@gmail.com
[2] Department of Geoscience and Petroleum, Faculty of Engineering, Norwegian University of Science and Technology, N-7031 Trondheim, Norway
[3] Maelgwyn Mineral Services Ltd., Ty Maelgwyn, 1A Gower Road, Cathays, Cardiff CF24 4PA, UK
[4] Department of Mining Engineering, Higher Education Complex of Zarand, Zarand 7761156391, Iran; khoshdast_hamid@yahoo.com
* Correspondence: ahmad.hassanzadeh@ntnu.no (A.H.); yqhe@cumt.edu.cn (Y.H.); przemyslaw.kowalczuk@ntnu.no (P.B.K.)

Abstract: This paper reviews recent developments in the fundamental understating of ultrafine (nano) bubbles (NBs) and presents technological advances and reagent types used for their generation in flotation. The generation of NBs using various approaches including ultrasonication, solvent exchange, temperature change, hydrodynamic cavitation, and electrolysis was assessed. Most importantly, restrictions and opportunities with respect to the detection of NBs were comprehensively reviewed, focusing on various characterization techniques such as the laser particle size analyzer (LPSA), nanoparticle tracking (NTA), dynamic light scattering (DLS), zeta-phase light scattering (ZPALS), and zeta sizer. As a key feature, types and possible mechanisms of surfactants applied to stabilize NBs were also explored. Furthermore, flotation-assisted nano-bubbles was reported as an efficient method for recovering minerals, with a special focus on flotation kinetics. It was found that most researchers reported the existence and formation of NBs by different techniques, but there is not enough information on an accurate measurement of their size distribution and their commonly used reagents. It was also recognized that a suitable method for generating NBs, at a high rate and with a low cost, remains a technical challenge in flotation. The application of hydrodynamic cavitation based on a venturi tube and using the LPSA and NTA in laboratory scales were identified as the most predominant approaches for the generation and detection of NBs, respectively. In this regard, neither pilot- nor industrial-scale case studies were found in the literature; they were only highlighted as future works. Although the NB-stabilizing effects of electrolytes have been well-explored, the mechanisms related to surfactants remain the issue of further investigation. The effectiveness of the NB-assisted flotation processes has been mostly addressed for single minerals, and only a few works have been reported for bulk materials. Finally, we believe that the current review paves the way for an appropriate selection of generating and detecting ultrafine bubbles and shines the light on a profound understanding of its effectiveness.

Keywords: nanobubbles; hydrodynamic cavitation; flotation; dynamic light scattering; bubble size

1. Introduction

Nanobubbles (NBs), also known as ultrafine bubbles, are extremely small (finer than 1 μm) and have several unique physical and physicochemical properties, making them very different from sub-micron (SMBs < 50 μm), micro- (MBs, 50–1000 μm) and conventional air bubbles (CBs, >1000 μm) [1]. They can be categorized into surface NBs (formed at solid–liquid interfaces), bulk NBs (exist in bulk liquid and are spherical with a typical diameter of 100–200 nm), and micro-pancakes (quasi-two-dimensional gaseous domains) [1,2].

The concept of NBs was first proposed in 1954 to explain the growth of NBs as gas nucleic during cavitation [3]. An analysis of the fast flotation kinetics claimed by the developed flotation cells in the early 1990s led to the initiation of a research program at McGill University to explore the role of gas nucleation and cavitation in flotation [4]. The research not only experimentally justified the benefits of applying the two-stage particle–bubble attachment model for the accelerated flotation kinetics but also developed the cavitation tube concept for generating an abundance of NBs in flotation to complete the requirements of the two-stage attachment model [4–6]. In 1997, improved flotation rates were reported when the NBs co-existed with CBs [5]. Later in 2000, the existence of NBs was reported using atomic force microscopy (AFM) by Lou et al. [7], when the first image of NBs on the hydrophobic solid surface was obtained. Since then, NB-adapted technologies have been applied as a problem-solving alternative for different challenges [7,8]. During recent years, liquids containing NBs have attracted attention in industry and academia because of their special properties and wide range of applications, such as nanoscopic cleaning [9], controlling slip in microfluidics [10], mineral flotation [11–14], chemical industries [15], and wastewater treatment [16]. Additionally, numerous studies have been conducted to investigate NB size, shape, surface charge properties, stability, and kinetics [17–19]. A historical overview of developments in theoretical and practical investigations regarding ultrafine bubbles is given elsewhere [20,21].

The generation of NBs is a complex physicochemical process that depends significantly on several parameters, including temperature, electrolyte concentration, dissolved gas content in solution as well as type and concentration of reagents [17,18,22–25]. Many methods, such as hydrodynamic cavitation [26], chemical reaction [27], ultrasonic oscillation [28], and electrolysis [29], have been used to generate either MBs or NBs. However, one of the rarely addressed critical points of using NBs is related to energy consumption and electrical expenses of their generators. In practice, the high energy consumption, installation inconvenience and maintenance difficulty encountered in ultrasonic and electrolysis methods have prevented them from being used in flotation [30]. Among these methods, hydrodynamic cavitation is considered the most promising method for large-scale mineral flotation applications due to its simple design and high throughput [31–35].

Over recent decades, a number of bubble size-measurement techniques have been developed, including X-ray techniques [36], optical microscopic and photographic methods [37], laser pulse methods [38], fluid dynamics methods [39], and image analysis [40]. Although these methods have been widely applied to characterize NBs, they have several obvious disadvantages: time-consuming data processes, requirement for a low bubble concentration, and a transparent barrier required for image acquisition [41]. Therefore, using laser diffraction-based technologies, e.g., laser particle size analyzer (LPSA), nanoparticle tracking analysis (NTA), and dynamic light scattering (DLS) for measuring the bubble diameter have become the preferred research techniques [42].

In the last two decades, the use of NBs has increasingly driven a lot of attention towards the mineral processing field because of their high gas solubility [23], high surface area [43], long lifetime [44], high concentration, improved hydrophobicity of solids [45], and extensive contact angle [14]. Additionally, it is now proven that they enhance recoverability and kinetics of flotation by increasing hydrophobicity of minerals, reducing reagent consumptions, increasing flotation selectivity of the desirable particles [46,47], and acting as a secondary collector [11–13]. In flotation, due to a specific movement of NBs in the liquid, they more easily colloid and attach to the surface of fine and ultrafine particles. Through this, NB-coated fine particles can be easily attached to the CBs and recovered [48–50]. Figure 1 shows NBs and CBs attaching to fine and coarse particles in flotation with two different mechanisms [51]. The ultrafine bubbles preferentially nucleate at the surface of hydrophobic particles [5] because the work of adhesion between a solid particle and water is always smaller than the work of cohesion of water. Furthermore, the work of adhesion decreases with increasing the solid surface hydrophobicity measured by the contact angle. NBs can nucleate on ultrafine particles without the need for collision, which is often the

rate-determining step in the froth flotation for ultrafine particles (<20 μm) [52,53]. Coarse particles attach more easily to CBs in the presence of NBs. Although nano-bubbles do not have sufficient buoyancy force to float coarse particles by themselves, the surface of a coarse particle coated with NBs is more hydrophobic than that without NBs. The wetting film separating the colliding CBs and NBs is more unstable than the film between the CBs and coarse particles. So, bubble–particle attachment and water film rupture can be accelerated in the presence of NBs [26,34,54].
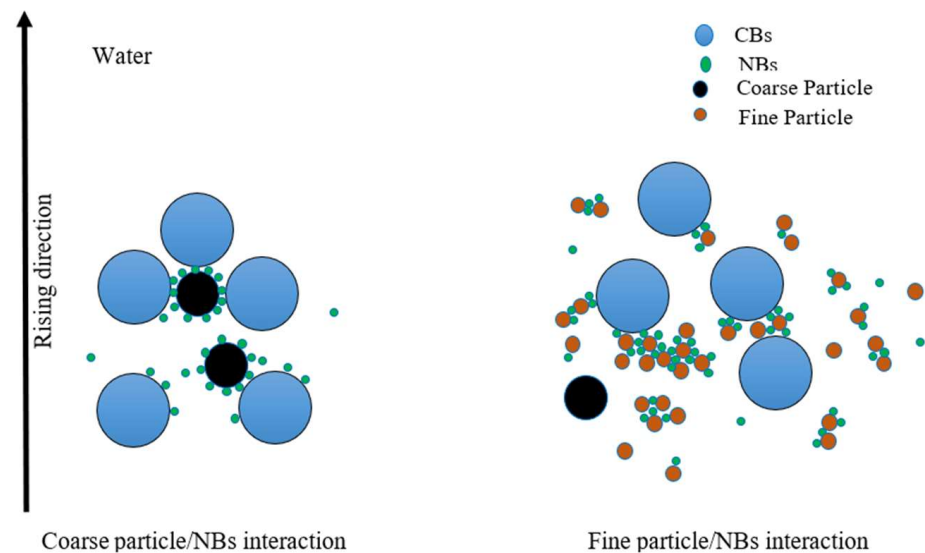

Figure 1. Representation of possible mechanism for coarse (**left**) and fine (**right**) particles floating in the presence of CBs and NBs.

NB-assisted flotation processes have provided great benefits to conventional flotation systems, as proven for coal [54–57], shale [24,58–60], quartz [61–63], scheelite [32], and chalcopyrite [64]. Despite a wide range of experimental studies, pilot- and industrial-scale applications are still very limited [65]. Further, most of the studies reported in the literature were conducted on single mono-minerals, while NB-assisted flotation application to actual ore samples has been relatively overlooked [5,26,53,60,61,64,66,67]. Figure 2 displays a number of scientific articles published and indexed by the Web of Science from 1993 to 2021 in the scope of NBs and their application in flotation. As seen from the graph, researchers are nowadays paying great attention to assessing NB-assisted flotation processes.

NBs can be generated by several methods, as shown in Figure 3. One of the important issues in the extended market is the production of NBs by simple, cheap, stable, and scalable methods [68]. Several companies in the USA, South Korea, Canada, and Japan have produced such bubbles by special methods containing cavitation chambers, electrolysis, shear planes, pressurized dissolution, and swirling fluids in a mixing chamber [69]. A significant number of works focused on bubble generation and properties after 2000, initially reported by Kim et al. [70]. Later, in 2007, Kikuchi and colleagues [29] generated NBs by electrolysis. NBs were produced by sonication of a perfluorocarbon gas by adding some surfactants, as reported by Oeffinger and Wheatley [71]. The formation of NBs in a closed cuvette by increasing the temperature was investigated by Najafi et al. [18]. Ultrafine bubbles were later generated by the injection of gas (N_2, CH_4, and Ar) into distilled water solution by Ohgaki et al. [72]. They reported that the concentration of NBs was 1.9×1016 bubbles per dm^3, and they remained stable for up to two weeks. The generation of NBs using a multiphase pump was studied by Etchepare et al. [73]. The results showed that the bulk NBs were stable for over 60 days, with no decrease in their concentration and mean size. Nazari et al. [12] studied NBs generated with different reagents in water by hydrodynamic cavitation. Bulk NBs generated with oxygen and air in the water and counter flow hydro-

dynamic cavitation was studied by Michailidi et al. [74]. The presence of OH radicals in low concentration was confirmed for all NBs samples.
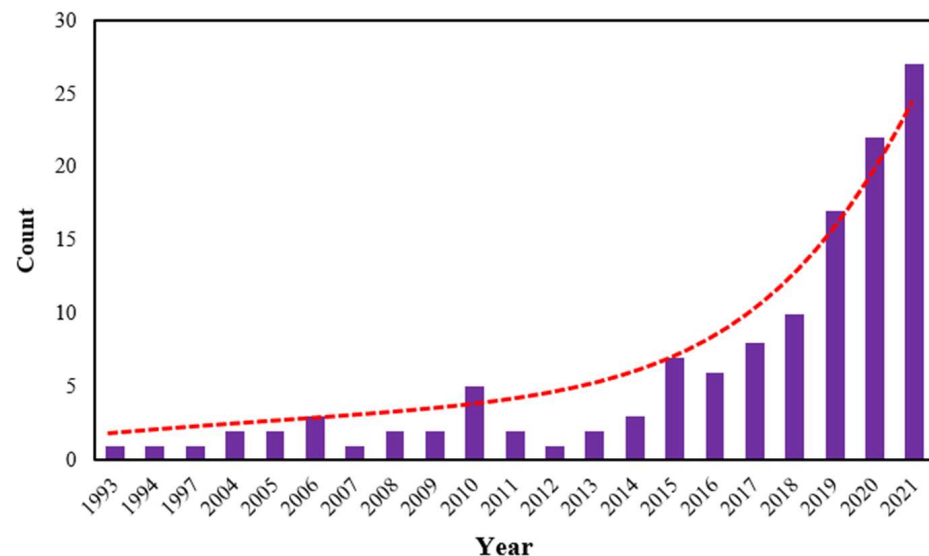
Figure 2. Number of manuscripts published in literature on application of NBs in flotation (from 1993 to 2021) (calculated based on the Web of Science data).
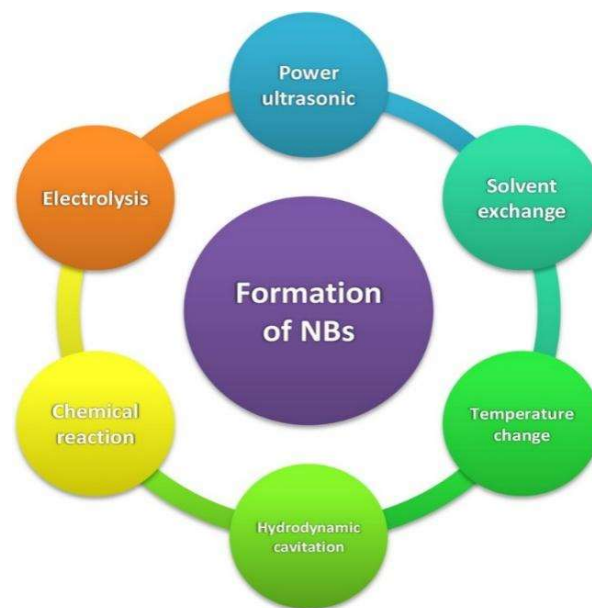
Figure 3. A schematic overview of commonly applied techniques for producing NBs.

Although NBs play a vital role in flotation of fine, ultrafine, and coarse particles, previous practical studies have mainly focused on the ultimate flotation performance and its kinetics in the presence/absence of NBs. A few review papers have recently highlighted the impact of NBs in flotation [75–78]. Their focus was mainly on the fundamental aspects of bulk NBs and their characteristics, however, to the best of the author's knowledge, there is a lack of thorough review on advancements in generators and detection methods of NBs as well as the effect of reagents on the production of NBs and their application in flotation. Therefore, the present paper reviews recent advances in these areas. In the first part of this paper, generation methods, detection techniques, and their accuracies are discussed. Commonly used reagents for the production of NBs are described in more detail. In addition, the effect of reagents on the flotation process is discussed. The final part is

focused on the application of NBs in mechanical and column flotation. We believe that the data and conclusions that are driven by this study will guide researchers towards profound understating, and may aid them to realize NB-assisted flotation systems in full scales.

2. Generation Techniques

2.1. Power Ultrasound

A commonly used approach for generating bubbles is via acoustic methods, which are relatively simple and applicable in large liquid samples of optically non-accessible media [79]. Ultrasound generators are compact, simple in operation, have a short generation time, and are contamination-free. Furthermore, the number of bubbles can be controlled by an appropriate selection of ultrasonic frequency and power [79]. For example, Leroy and Norisuye [80] proposed that ultrasound is an ideal tool for investigating the existence of bulk NBs because (i) it is sensitive to minute quantities of gas; (ii) it allows one to determine the bubble size distribution; and (iii) it discriminates unambiguously between gaseous and solid/liquid inclusions. Nevertheless, analyzing literature data clarifies that there is generally no unified statement regarding the creation of NBs by acoustic waves. Such contradiction is mainly related to the utilization of different experimental apparatus, studied parameters, and various purposes of the experimental setups [81]. Further in-depth information regarding the sonication parameters and their effects on the bubble size distribution can be found elsewhere [81]. Chen et al. [82] classified the ultrasonically created bubbles into three zones based on the ultrasonication time and frequency, i.e., low (20–50 kHz), medium (200–1000 kHz), and high (>1 mHz). They found that the NBs were unstable at low frequencies, owing to the transient cavitation effect, while the medium range of frequency was selected as the optimum range for acoustic-assisted flotation processes regarding the formation of stable NBs. Power ultrasound (20–100 kHz) penetrates into the medium and creates acoustic cavitation bubbles [83]. In this method, the pressure sharply decreases below the saturated vapor pressure and leads to considerable dissolving of air and its conversion to bubbles [28,84]. Miastkowska et al. [85] showed that NBs form from bubble nuclei when the ultrasound irradiates into water, and grow to resonance size under acoustic pressure fluctuations and collapse (acoustic cavitation). Thus, ultrasound's time, frequency, and power substantially impact the size of acoustically generated bubbles. Additionally, Cho et al. [17] concluded that the effective diameter of NBs generated by ultrasound in pure water was maintained at 750 nm, without significant change within one hour. In addition to the creation of ultrafine bubbles, a positive effect of ultrasonic-assisted flotation either as a pretreatment or simultaneous process has been extensively reported by many researchers on a wide variety of metallic and non-metallic minerals [83,86,87]. Scientists partially related such improvements to the presence of NBs leading to an increase in the hydrophobicity of solid surfaces (expressed as a water contact angle) [88,89].

2.2. Solvent Exchange

One of the simplest methods used to create ultrafine bubbles is solvent exchange, which applies an exchange of two solutions with different gas solubilities such as ethanol and water. This method is usually used for the production of NBs on a laboratory scale [7,22,75].

The solvent-exchange process includes a few steps, shown in Figure 4, where at first, a hydrophobic substance should be contacted with water. Then, ethanol replaces water, and NBs are formed and cover the substance's surface. Gas molecules do not diffuse into the atmosphere and stay in the water during the replacing water of with ethanol. Organic solvents such as ethanol, methanol, and 2-propanol can be applied to produce NBs [90,91]. Because the air has a higher solubility in ethanol than water, the exchange process leads to gas supersaturation, and consequently, NB nucleation. These NBs form a huge number of interfaces in the solution. These interfaces can cause the directed arrangement of ethanol molecules due to their amphiphilic nature [91]. Further, other methods such as exchanging cold water against warm water and ethanol solution against salt solution have been applied for producing NBs [75]. Ethanol–water exchange was used for the first time on the surface of

mica by Lou et al. [7] to generate ultrafine bubbles. Some researchers found that the number of NBs was enhanced with an increase in the alcohol concentration up to 70%, and above this concentration, the bubbles disappeared [92]. Xiao et al. [91] applied molecular dynamic (MD) simulations for predicting the NBs generation by the solvent-exchange method. They showed that there is an interface between exchanging solvents with different gas solubilities, and the interface gradually moves towards the substrate, forming NBs in the bulk solution and/or on the hydrophobic solid surface.
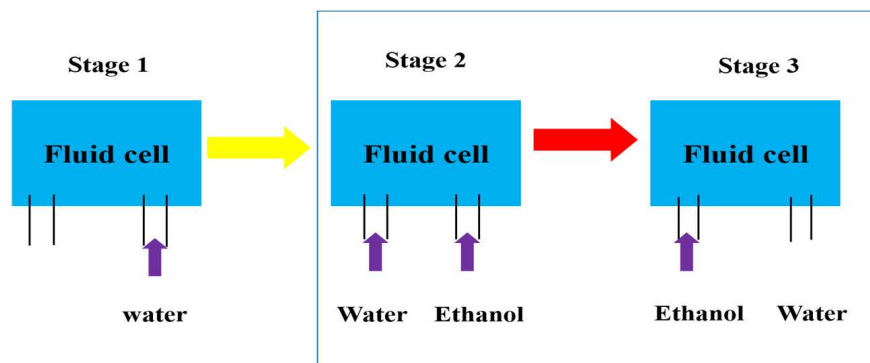
Figure 4. A stepwise process of alcohol–water exchange method and generation of ultrafine bubbles. Reprinted with permission from [68]. Copyright (2015) by the American Physical Society.

Although the solvent exchange is used for generating bubbles, the exact mechanism of processing the gas saturation is yet unknown. Furthermore, the solvent-exchange method cannot control bubble formation precisely because several factors such as the exchange rate, liquid shear, saturation level of gas, and flow boundary conditions, cannot be controlled during the experiments [91].

2.3. Temperature Change

Another technique for producing ultrafine bubbles is the temperature difference method. Changing temperature is one of the important physical and chemical factors related to bubble generation at the solid–water interface [93,94]. In this method, the gas solubility in water and heat diffusion reduce due to increased temperature. Through this, water becomes supersaturated with air, and releasing gas induces the production of fine bubbles on the solid surface [22,75]. Some researchers have reported that the increase in the liquid temperature leads to the formation of in situ NBs [22]. They showed that NBs generated during immersion and at high-water temperatures remain stably on the surface at low water temperatures. Moreover, such bubbles were sensitive to the cleaning process used to prepare the substrates [22]. Zhang et al. [95] and Yang et al. [22] showed that when the temperature was enhanced to 30 °C, the density of bubbles was enhanced very slowly, but was boosted sharply when the temperature increased further (Figure 5). They also indicated that the generated bubbles did not disappear when the water cooled down to ambient conditions, and they were remarkably stable.

2.4. Hydrodynamic Cavitation

In recent years, one of the most critical methods for generating NBs has been hydro-dynamic cavitation [5,12,53]. This is the process of creation and growth of gas bubbles in a liquid due to the rupture of either a liquid–liquid or a liquid–solid interface under the influence of external forces [96]. In other words, when rapid changes in pressure in a liquid occur in places where the pressure is relatively low, vapor-filled cavities are formed, and this phenomenon is called cavitation [32,34,97].
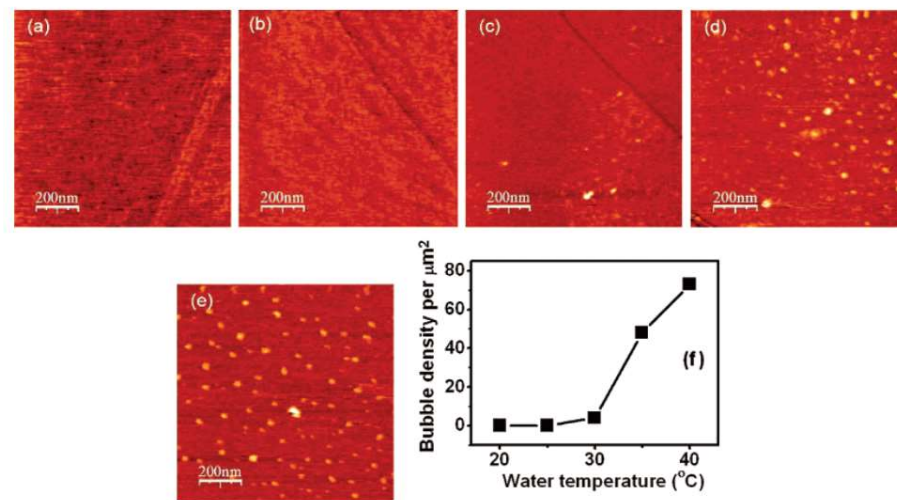
Figure 5. AFM images at different water temperatures in intervals of 5 °C:20–40 °C (**a–e**). (**f**) The NB density as a function of water temperature. Reprinted with permission from [22].

The first study of cavitation was carried out in the 1710s, but the term cavitation was introduced in 1895 by Thornycroft and Barnaby [98]. The first stage of cavitation is defined as nucleation, which is the formation of cavities. In this process, the liquid structure is ruptured to form a hole by external forces. Additionally, rupture starts at a weak location where the intermolecular forces approach zero [99,100]. The nucleation of a bubble on a particle surface increases bubble–particle collision, which is often a rate-limiting step in flotation with CBs. Hence, cavitation and gas nucleation provide a suitable mechanism for the collection in flotation [101]. Hydrodynamic cavitation is well-described by Bernoulli's equation [5]:

$$P + \frac{1}{2}\rho U^2 = C(constant) \tag{1}$$

where U is the water flow velocity at a point where the pressure is P, and ρ is the liquid density.

Cavitation number (K) is normally used for calculating the onset of cavitation in either equipment or components with flow constrictions, and is defined as follows [4]:

$$K = \frac{2(P_{min} - P_{vap})}{\rho \cdot v^2} \tag{2}$$

where P_{min} is the minimum pressure occurring in the vicinity of the restriction, P_{vap} is the vapor pressure of the liquid, ρ (kg/m^3) is the density of the liquid, and v (m/s) is the flow velocity through the restriction. The cavitation phenomenon occurs when the cavitation number is less than 1.5 [102].

Cavitation is affected by many factors, which include geometric parameters, operational conditions, dissolved gas content, reagent concentrates, and the addition of solids [101,103]. A venturi tube is typically used as a hydrodynamic cavitation device (Figure 6). The liquid in the cylindrical throat is higher in flow velocity and lower in pressure than the liquid in the entrance cylinder, resulting in cavitation. The differential pressure between the entrance cylinder and the cylindrical throat measured by the manometers is indicative of cavitation behavior [5,96,101]. Different designs of cavitation tube technologies have emerged and become commercially available for laboratory research, flotation machines, and commercial flotation operations. For example, Eriez Manufacturing Co., (Erie, PA, USA) has sold more than 200 flotation columns using CavTubes for sparging, and has retrofitted many other columns with the cavitation tube technology [104].
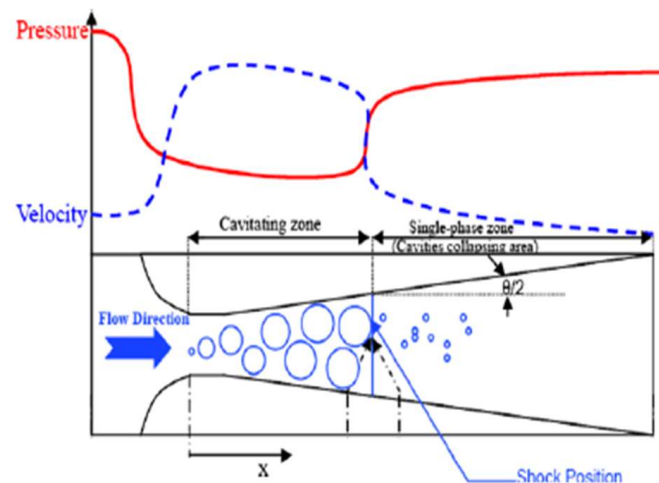
Figure 6. Schematic diagrams of NB generator based on hydrodynamic cavitation [103].

Some companies, such as Canadian Process Technologies (CPT), Coalberg seam coal in West Virginia [59], CSIRO Energy Technology, and Novatech Consulting [105], have applied high-shear cavitation to improve flotation of fine coal, iron ore, phosphate, fluorite, niobium, feldspar, mica, and molybdenum. They illustrated that recovery of fine and coarse particles was low by CBs, which was improved by applying hydrodynamic cavitation. Some researchers have used this mechanism as a pulp pretreatment method before flotation [6,51,64,106]. Other studies have employed it in flotation separation processes; the tests were carried out in mechanical and column flotation cells [13,51,53,107,108]. Additionally, recent tests have shown the potential of its application to recover/remove residual bitumen from oil–sand mature fine tailings [102].

Some researchers have also investigated the effect of different types of gases (e.g., air, O_2, N_2, Ar, and CO_2) on NBs generation [97,103]. The results confirmed that the sizes of ultrafine bubbles were well-correlated to the gas solubility in water. Indeed, larger bubbles were obtained with gas of a higher solubility, accompanied by more ultrafine bubbles generated. Li [109] reported that a linear correlation was found between the volume of generated cavity bubbles and air saturation pressure, further confirming that NBs generation and stabilization are proportional to the dissolved gas concentration.

2.5. Electrolysis and Chemical Reaction

An alternative method to produce NBs is water electrolysis. In this technique, oxygen and hydrogen bubbles can be generated at the hydrophobic surface–water interface by producing oxygen and hydrogen gases at the electrolysis electrodes when the surface acts as a negative electrode. Changing voltage and reaction time affects the formation, growth, and size of NBs. The type of gas applied is also an essential factor in controlling the generation and properties of NBs. The results illustrated that the number of oxygen bubbles generated was substantially smaller than the hydrogen ones, because oxygen solubility in water is approximately two times the solubility of the hydrogen during the electrolysis process [110]. Further, oxygen bubbles are more stable than air bubbles, which in turn are more stable than other NBs [46]. This method is mainly applied in electro-flotation techniques [110,111].

The supersaturation of dissolved gas can further produce bubbles by chemical reactions, which liberate a gaseous species. This can be applied as a potential method for generating ultrafine bubbles (Figure 7). For example, carbon dioxide generated by mixing acid with carbonate was applied in a reactive flotation technique [100,112]. In this method, the concentration of reactants and the solution conditions were controlled by the rate of a chemical reaction that can be enhanced using catalysts. Thus, gas supersaturation by the chemical reaction provides relatively appropriate conditions for the generation of NBs. Some researchers have investigated the electrochemical nucleation of bubbles on solid nano-electrode surfaces [113,114]. The reduction of protons in acidic solutions [113] and

oxidation of N_2H_4 [114] and H_2O_2 [115] generated gaseous products (hydrogen, nitrogen, and oxygen). In another study, the chemical reaction between ammonium chloride and sodium nitrite created bulk nitrogen NBs with diameters of 200–300 nm [116]. They concluded that these bubbles formed only when they were trapped between two carbon films.
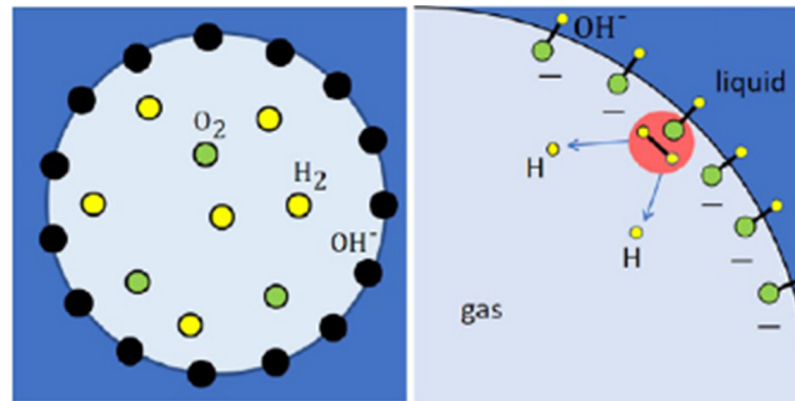
Figure 7. Schematic overview of chemical reaction happening on the bubble surface. Reprinted from [27]. Copyright (2022), with permission from Elsevier.

3. Bubble Size-Measurement Techniques

One of the important physical properties of bubbles is their size, which can be measured under various conditions and descriptions along with the gas hold-up and velocity [117]. Several methods are available for the detection of bubble size, including optical methods such as high-speed photography [118,119], image analysis [120], and electrical impedance [121,122], as well as acoustical methods [108,123–125]. Table 1 presents the generic methods applied to measure CB sizes in froth flotation, and detailed information regarding the modern techniques can be found elsewhere [126]. These commonly used methods are not capable of measuring ultrafine bubble sizes because of their too-small diameters [69].

Table 1. Comparison of three major techniques to measure the size of CBs.

Analysis Technique	Size (μm)	Analysis Speed	Data Output	Advantages and Disadvantages
Acoustical methods	34–1200	Fast and highly automated	Size, size distribution	Available in non-transparent media. High cost and limited data output.
Light scattering	<100	Fast and automated	Size, size distribution	Small range, limited output and generally used in backlighting illumination
Photographic	>50	Slow and manual	Size, size distribution, rise velocity, shape analysis, formation process	Available for obtaining more information, modifiable, relatively low cost, viscous liquids.

Recently, several methods have been used for measuring the NB size distribution, such as the laser particle-size analyzer (LPSA) [34,64,97], nanoparticle tracking analysis (NTA) [28,127,128], zeta sizer [61], dynamic light scattering (DLS) [129,130], and zeta-phase light scattering (ZPALS) [46], direct measurement by optical microscopy and indirect measurement by dissolved oxygen (DO) reverse estimation [69]. Table 2 summarizes studies that applied these techniques for measuring the presence and size of NBs on various solid surfaces. Additionally, the studies show that the distribution and size of NBs depend on the system design and various operational conditions [7].

Table 2. Comparison of three major techniques to measure the size of CBs.

Size Analyzer	Equipment	Material	Refs.
LPSA	Venturi tube	Coal	[107]
	Venturi tube and static mixer	Coal and phosphate	[11,24,131]
	Venturi tube and the static mixer	Coal	[53]
	Static mixer- venturi tube	Coal	[55]
	Venturi tube	Chalcopyrite	[64]
	Venturi tube	Coarse quartz particles	[34,51]
	Venturi tube and static mixer	Coal	[101]
	Venturi tube	Phosphate ore	[60,132]
	Venturi tube	Sub-bituminous coal	[56]
	Venturi tube	Hematite	[133]
	Venturi tube	Coal	[35]
	Hydrodynamic cavitation	Coal	[134]
DLS	Venturi tube	Fine silica and zinc sulphide	[5]
	Porous membrane system	UN *	[129]
	Hydrodynamic cavitation	Coal	[135]
NTA	Needle valves	Ferric hydroxide	[73,127]
	Depressurization of DI water	Quartz and apatitic minerals	[63]
	Venturi tube	UN *	[33]
	Venturi tube	Muscovite	[13]
	Ultrasonic	Mica	[86]
	Decompression method (Vacuum drying oven)	Kaolinite	[136]
	Depressurization with a gas vent	Platinum nanoparticles	[137]
Zetasizer	Steel needle valve	Quartz	[61]
	Flow constrictor (needle valve)	Quartz	[138]
	Venturi tube	Scheelite	[32]
	Venturi tube	Scheelite	[106]
	Venturi tube	Diaspore and kaolinite	[14]
	Venturi tube	UN *	[74]
ZetaPALS	baffled high intensity agitation (BHIA)	UN *	[46]
	High speed agitator	Alumina and silica	[139]
	Venturi tube	Coal	[45]
AFM	Solvent-exchange	Graphite	[140]
	Blowing N_2 and CO_2 gas into deionized (DI) water	Pyrite	[141]
	Temperature rise	Muscovite	[94]
	Venturi tube	Au, Pb	[142]
Beam Reflectance Measurement (FBRM)	Venturi tube	Subbituminous coal	[143]
Camera	Ultrasonic	Zinc ore	[83]
high-speed camera system	Venture cavitation sparger	Coal	[144]
A 405 nm laser beam	YBM Fubby (cavitation bubbles and vortex flow)	UN *	[25]
High speed camera	Venturi tube	Apatite	[57]
Photocamera- Microscope	Air-in-water microdispersion generator	Glass beads	[145,146]
UN *	Temperature rise	Bitumen	[147]
	High-speed venturi nozzles	Platinum Group Metal (PGM) tailings	[148]
	Temperature rise	Coal	[149]
	Ultrasonic cavitation	Coal	[67]
	Ultrasonic cavitation	Rutile	[150]
	Venturi tube	Bitumen	[151]
	Venturi tube	High-ash coal	[152]
	Venturi tube	Apatite ore	[153]
	Venturi tube	Pb–Cu–Zn sulfide ore	[154]

* UN: unknown or not mentioned in the manuscript. For the type of mineral, this term might suggest the presence of NBs only in bulk solution.

Among available techniques for measuring NB size, LPSA is the most frequently used [155]. Measurements with this device can be described based on the Mie's theory, considering a refractive index of 1.0 for air NBs and 1.33 for water [51,156]. In recent years, this technique has been applied to measure NBs in flotation of different solids such as coal,

phosphate, hematite, and quartz [12,56,60,133]. LPSA has many advantages, such as quick measurement (from two seconds to ten minutes), being easily operated, its repeatability for large numbers of entities, and control of the dispersion process. The limitation of this technique is the assumption of shape sphericity, which is not valid neither for particles nor for bubbles. Non-spherical entities can be equivalent to a combination of a series of spherical ones with different sizes, which leads to a higher proportion of tiny entities, and the whole distribution becomes broader [157–159].

A nanoparticle tracking analysis (NTA) is a method for the direct and real-time visualization and analysis of NBs in liquids [127]. This method can be used to detect concentration, zeta potential, fluorescence, and particle size range of approximately 10 nm to 1 μm in liquid suspension, and requires fast computer systems that are able to cope with the computationally intensive video analyses in reasonable time frames. This method was initially utilized almost 25 years ago, but bubbles' size measurement can be considered relatively new to the market [160,161]. A combination of an ultra-microscope and a laser illumination unit must be used to estimate bubble diameters accurately. More detailed information regarding the measurement mechanism can be found elsewhere [162,163]. Some researchers have applied NTA as a suitable method for analyzing NBs [33,63,127].

Dynamic light scattering (DLS) is also a well-established method for the measurement of particle and bubble size distributions in colloidal suspensions and emulsions typically in the sub-micron region (lower than 1 μm). Some researchers have applied this technique for bulk and surface-attached NBs [5,127,135]. In a DLS experiment, a sample is illuminated with a laser beam and the temporal fluctuations are analyzed at a known scattering angle of θ by means of the intensity of photon autocorrelation function. The scattering signal is either directly received by the detector or superposed by a reference beam [164,165]. This method has several advantages such as (i) the experiment duration is short and it is almost fully automatized, so that for routine measurements, extensive experience is not required; (ii) this method has modest development costs; (iii) and it is possible to obtain absolute measurements of several parameters of interest, such as molecular weight, a radius of gyration, and diffusion constant [160,166]. However, this technique has also specific application limits that restrict its usage, for reasons such as (i) being affected by several instrumental parameters; (ii) DLS signals allow for only a rather limited resolution of size distribution, and the results are considerably affected by the employed algorithms; (iii) the optical models typically rely on the assumption of spherical entities, that is rarely met in real-life analyses; (iv) and DLS alone does not provide chemical information to distinguish gas NBs from either particles or droplets [164,165].

A zetasizer is also often applied for the measurement of ultrafine bubble size. Its main features are automatic optical alignment prior to testing, set measurement positions, and precise temperature control, which make measurements extremely repetitive and accurate [167]. The zetasizer nano series uses a process called DLS for size measurements. This is achieved by irradiating entities with a laser to analyze fluctuations in the light strength of scattered light. For DLS, an important feature of the Brown's motion is that small bubbles move quickly and large ones move slowly. As bubbles move around, the constructive and destructive phase overlay of scattered light causes bright and dark areas to increase and decrease in a light-strength manner—or in another way, the light appears to fluctuate. It eventually measures the speed at which light strength fluctuates and is then used to calculate the bubble size. Additionally, this method uses a process called static light scattering (SLS) to measure the molecular weight to obtain molecular characteristics in a solution [32,106,168].

The atomic force microscopy (AFM) technique has recently been utilized to measure the bubble size on the solid surface. Its advantage is the incomparable 3D resolutions of surface NBs. In particular, the contact angle of NBs can be extracted from the cross-sectional profile of NBs in the AFM image. However, one of several disadvantages of AFM is the inevitable perturbation of the examined sample by the probe. Thus, one main concern was that the bubbles were not present on the surface until the surface was perturbed by

the AFM probe. After several complementary measurements, it was proven and generally accepted that the presence of surface nano-bubbles was not the consequence of the tip perturbation [68,169].

Another method to measure the bubble size is optical microscopy by transmission and Scanning Electron Microscopy (SEM). Cyro-EM or freeze-fracture electron microscopy has been applied as a promising method for the observation of NBs and has shown high resolution and the capability of providing direct evidence [170,171]. Some researchers have shown that in the freezing process, bubbles may agglomerate and coalesce [22]. Although this method has limitations such as being slow, manual, and also that obtaining statistically significant data can be extremely time-consuming, it is easily modifiable and relatively low cost, applicable for viscous liquids, and its use in developed lab view-based bubble analysis processing has led to analysis tailored to specific requirements [159,172]. Furthermore, this method can accurately measure the size of a single bubble but cannot measure a large number of bubbles at the same time. Additionally, when the bubble becomes smaller, progressively more time is required to adjust the light intensity and focus on the individual bubbles [69].

Karpitschka et al. [173] non-invasively investigated NBs nucleation on glass using interference-enhanced reflection microscopy. The evidence of surface NBs using total internal reflection fluorescence microscopy (TIRF) with dye-labeled NBs was studied by Chan and Ohl [174]. The methods investigated by these researchers do not provide evidence for the gas content and have diffraction-limited lateral resolution [174].
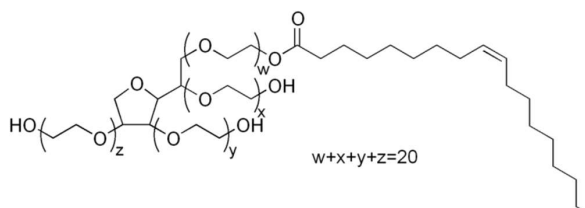
4. Commonly Used Reagents for Producing NBs

Numerous studies have focused on the influence of different types of reagents on the physiochemical characteristics of NBs. These reagents may be ionic and nonionic surfactants, salt and electrolyte solutions, and mixtures thereof. In flotation, different surface-active substances, mainly frothers, are used to generate bubbles and stabilize the froth [126,175]. The features of generated bubbles are also affected by temperature, airflow rate, pH, and pressure. Principally, the stabilizing role of reagents is due to their ability to reduce the surface energy and surface tension of the air/water boundaries [50].

Although it is well-known that the structure and other physicochemical properties of surfactants significantly influence the characteristics of bubbles in aqueous solutions, a few papers have surveyed the real effect of surfactants on the production of NBs and their application in flotation. Generally, it is well-demonstrated that using a suitable frother can reduce the size of bubbles by between 13 and 35% [176]. Table 3 presents a summary of the physicochemical properties of surfactants used for NBs generation. Details on various physicochemical characteristics of flotation frothers can be found elsewhere [126,177,178].

Table 3. Physiochemical properties of surfactants used for NBs generation.

Surfactant	Formula	Structure	MW (g/mol)	HLB	Used by
Methyl isobutyl carbinol (MIBC)	$(CH_3)_2CHCH_2CHOHCH_3$		102.17	6.00	[11,24,26,50,53,60,97]
Pine Oil (PO)	$C_{10}H_{18}O$		154.25	5.40	[26]
Dipropylene glycol (DPG)	$C_6H_{14}O_3$		134.17	9.30	[26,50]
Dodecylamine (DDA)	$CH_3(CH_2)_{11}NH_2$		185.35	10.70	[13,26]
Flotigam EDA 3B *	$[R–(O–CH_2)_3–NH_3] + CH_3COO^-$ **	Commercial cationic alkyl methyl ether monoamine	195.00	NA ***	[63,179]
Dodecylamine hydrochloride (DAH)	$C_{12}H_{28}ClN$		221.81	NA	[18]
PEB70 *	$CH_3(CH_2)_3O(C_2H_4O)_nH$		~250	NA	[103]
Dodecyltrimethyl ammonium chloride (DTAC)	$C_{15}H_{34}ClN$		263.89	NA	[180]
Sodium dodecyl sulphate (SDS)	$CH_3(CH_2)_{11}SO_4Na$		288.37	40	[18,179–181]
FLO-YS-20 *	Collector–frother based on fatty acids	Straight structure with long hydrocarbon chain	>300	NA	[60,103]
F507	$H(C_3H_6O)_{6.5}OH$		425.00	8.63	[11,24,53,97]

Table 3. *Cont.*

Surfactant	Formula	Structure	MW (g/mol)	HLB	Used by
Polysorbate 80 (Tween 80)	$C_{64}H_{124}O_{26}$		1310.00	15.00	[181]

w+x+y+z=20

* Proprietary formulation. ** R is a hydrocarbon chain with 10 carbons. *** Not available.

Studies by Nazari et al. [182] and Nazari and Hassanzadeh [26] demonstrated that NBs generated in the presence of dodecyl amine (DDA) are more stable than pine oil (PO), MIBC, and dipropylene glycol (DPG). According to the results, the mean size of generated NBs was orderly categorized as DPG < DDA < MIBC < PO and DPG < MIBC < PO < DDA. These results were ascribed partly to the surface activity of surfactants and partly to the improved surface charge of NBs and increased hydrophobicity of the solid surface. The same results were reported by Yasui et al. [79] and Zhou et al. [13], as they demonstrated that some DDA molecules can adsorb on the NBs surfaces, thus making them more positively charged. In other studies, it was reported that the effects of NBs generated by MIBC, PEB70, and FlO-YS-20 were very important in flotation [60,103]. Based on their studies, the median size of NBs for various frothers was obtained in accordance with the order FlO-YS-20 < MIBC < PEB70. The generation of NBs with smaller size distribution by MIBC compared to PEB70 was due to the greater reduction in surface tension of the liquid and greater foamability of this frother. They also investigated that NBs had a major role in the gas holdup, and fine bubbles at a given gas holdup decreased the frother consumption. Moreover, FlO-YS-20, which is a type of fatty acid, generated finer bubbles than MIBC at lower concentration of reagents [60,103].

The role of MIBC and F507 frothers in flotation of fine coal particles using NBs was studied by Sobhy and Tao [53]. They revealed that F507 produced finer bubbles than MIBC (about 20% smaller). This is because the surface tension reduction by F507 is more significant in comparison to MIBC. Their results were consistent with those formerly reported by Fan et al. [11,24,97]. Calgaroto et al. [179] used a mixture of sodium dodecyl sulfate (SDS) and a commercial cationic alkyl methyl ether monoamine (Flotigam EDA 3B) as the surfactant solution in their studies. They showed that highly charged and small NBs (approximately 150–180 nm) were obtained in the presence of surfactants ($10-4 \text{ mol/dm}^3$). Similar results were reported by other researchers [18,63,180]. Recently, Phan et al. [181] studied the effect of sodium dodecyl sulfate and polysorbate 80 (Tween 80) on the generation of CO_2 NBs in an aqueous system. They observed smaller diameter and higher zeta potential magnitudes of NBs in the SDS medium. These results were attributed to the increased CO_2 concentration and the decreased surface tension of the solution. However, NBs disappeared with the incorporation of Tween 80.

According to the results reported in the literature, it is observed that surfactants that have little tendency to interact with the particle surface produce larger bubbles than solidophilic surfactants. These surfactants include a variety of alcohols and ethers. The effect of these surfactants can be examined from the perspective of two useful terms: selectivity and frothing power [183]. There are several methods for classifying frothers in these two groups, the simplest of which is the use of molecular weight (MW) and hydrophilic–lipophilic balance (HLB) diagrams [184]. The position of the surfactants reported in Table 3 in the MW-HLB diagram is shown in Figure 8. In general, selective frothers are surfactants that have lower MW and HLB. These frothers are suitable for stabilizing small bubbles due to their lower frothing power and less surface activity, and as a result, they might improve the flotation of fine particles. In contrast, frothers with higher MW, due to the increased elasticity of the thin film of bubbles, keep the bubbles stable in larger dimensions, and therefore might be suitable for flotation of large particles [183,185,186]. A comparison of the results reported in the literature show that heavy surfactants such as PEB70 are not suitable to produce NBs. However, contrary results have been reported by other researchers [11,24,53,97]. Although many efforts have been made to interpret the effect of frothers on the size of MBs (generally coarser than 500 μm) [187,188] based on more efficient factors such as critical coalescence concentration (CCC), the issue needs more explorations in the field of NBs generation.
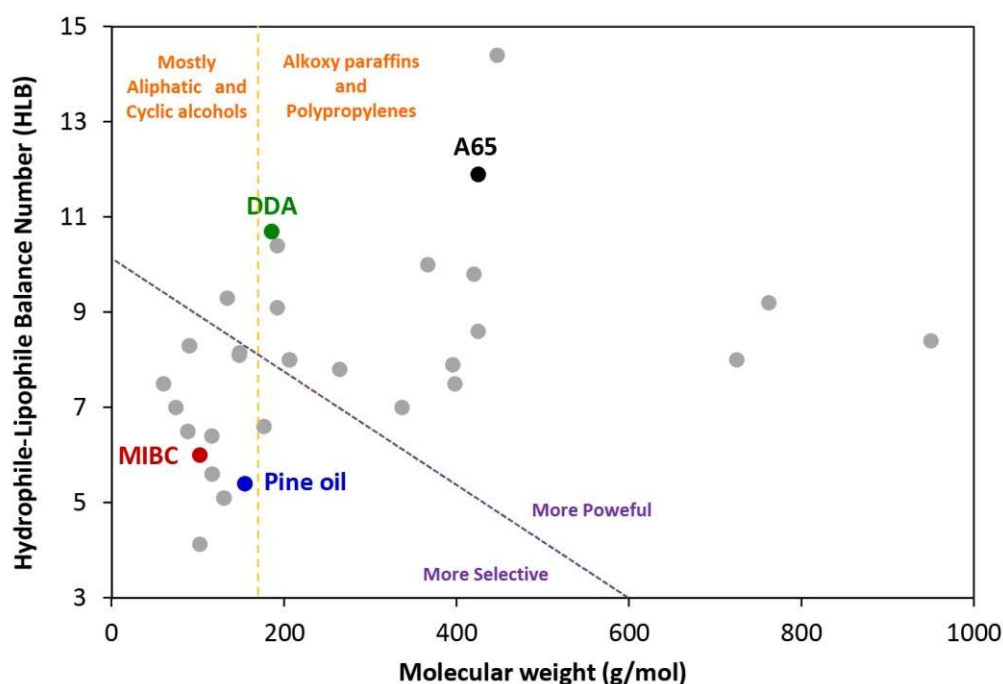
Figure 8. Classification of surfactants based on HLB–molecular weight diagram (drawn for HLB values < 15 and MW < 1000 g/mol; Grey dots correspond to other frothing surfactants reported in the literature [126,184].

The effect of solidophilic surfactants, such as DDA and FLO-YS-20, can be examined from two perspectives: film elasticity and ionic strength. Cho and Laskowski [189] found that the effect of frothers on the bubble size results from their ability to prevent bubble coalescence. The stability of such systems is determined by surface elasticity forces [23,189]. Comparing the structure of these solidophilic surfactants with more effective frothers such as MIBC and pine oil shows that these surfactants have a much simpler structure. Therefore, more molecules of these surfactants can be adsorbed at a certain surface area of bubbles and can improve the elasticity and stability of the bubble thin film by creating a more compact adsorption layer [190]. However, the dominant mechanism for improving the production efficiency of NBs in the presence of these surfactants can be attributed to the ionic strength of the surfactant in the aqueous system and its effect on the zeta potential of the NBs/particle system.

Many experimental techniques such as AFM [191], rapid cryofixation/freeze-fracture [192], neutron reflectivity measurements [193], dynamic light scattering [23], and optical visualization [173] have proven that NBs can be stable for a long time. The results illustrate that the type of surfactant can influence the stability, surface charge, and size of NBs [117]. The stability of NBs is affected by the type and number of polar groups, i.e., OH^- and H^+ ions, because the solution pH has an important role in the zeta potential and physicochemical features of NBs [194]. It is well-demonstrated that the surface of NBs is negatively charged due to the orientation of water dipoles at the air/water interface, and thus the selective adsorption of OH^- ions at the surface of the bubbles [70]. The type and concentration of surfactant molecules are the other important factors affecting the surface charge of NBs [179]. For example, Kim et al. [70] performed a detailed study on the effect of different types of polyoxyethylene methyl ether, glucopyranosides and polypropylene glycol surfactants on the zeta potential and surface charge of NBs. They showed that the zeta potentials of NBs in the presence of glucopyranosides with different lengths of alkyl chain and head group numbers were negatively charged in a wide range of pH conditions. Under acidic conditions, the surface charge of NBs was negative with polyoxyethylene dodecyl ether and positive in the presence of polyoxyethylene methyl ether, whereas polypropylene glycol provided a negative charge at the surface of NBs under alkaline conditions. They

also introduced two factors to explain the effect of surfactants on the surface charge of NBs: (i) the chemical characteristics of the nonionic surfactant's head group, and (ii) the polarity level of surfactant molecules [70]. They also demonstrated that basic ether linkages encourage the adsorption of H^+ ions where the molecules of polyoxyethylene nonionic surfactants tend to attach to the air/water interface under acidic conditions. Contrary to the common myth, glucopyranosides also showed similar overall trends with pH, while it was expected that the surface charge of NBs should be positive at acidic pH due to the higher ratio of oxygen to carbon. The fact behind this phenomenon (Figure 9) is that the acidic OH^- groups in competition with basic ether groups preserve HC ions in the bulk water phase during the adverse interactions between H^+ and OH^- functions. It was also observed that hydroxyl groups in glucopyranosides have no clouding effect on the structure of glucopyranosides, but their competitive adsorption with H^+ ions may be influenced by the surfactant polarity. These studies revealed that the zeta potentials and critical micelle concentration (CMC) of glucopyranosides with different alkyl chain lengths and glucose ring numbers were of the same order at given pH values. As shown in Figure 9B,C, the magnitude of the negative charge of the glucopyranoside molecules is directly proportional to their hydrophobicity. Generally, the surface charge of NBs is significantly influenced by the hydrophile–lipophile balance (HLB) number of the surfactant, such that polyoxyethylene dodecyl ethers with HLBs higher than 17 reveal negative zeta potential from pH 3 to 12. However, they suggested further studies to explore the possible relationship between HLB and the zeta potential and pH to find a predictable HLB point at which the positive surface charge appears [70].
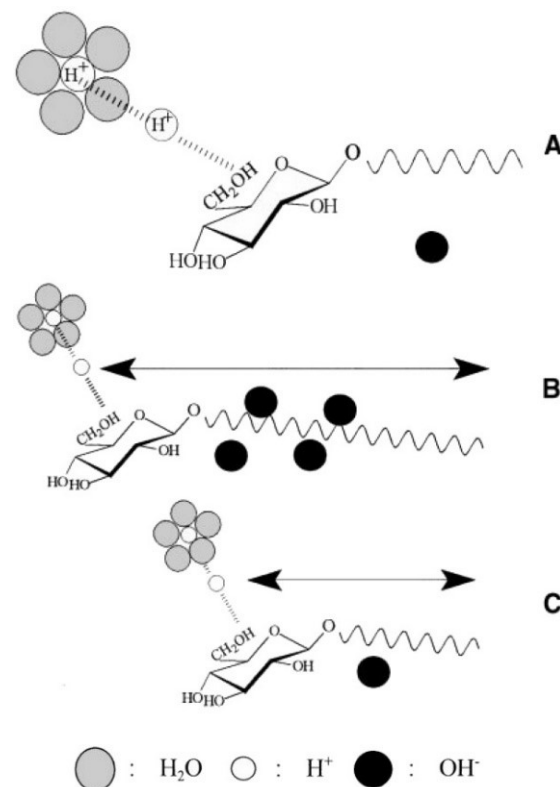
Figure 9. Proposed mechanisms of the air/water interface charging process: (**A**) Repelling of HC ions by OH^- groups of AG under acidic pHs, (**B**) enhanced adsorption of OH^- ions for highly hydrophobic surfactants, and (**C**) reduced interaction between anions and air/water interface for hydrophilic surfactants. Reprinted from [70]. Copyright (2022), with permission from Elsevier.

Calgaroto et al. [179] studied the effect of a commercial alkyl methyl ether monoamine with cationic character and SDS on the zeta potential of NBs. By comparing similar results reported by Najafi et al. [18] and Jia et al. [180], they concluded that in the presence of

cationic derivatives from amines, the positive surface charge of NBs reduced the rate of surfactant adsorption up to the isoelectric point (IEP), after which the negative charge was significantly neutralized. Conversely, SDS significantly neutralized the positive surface charge of NBs under acidic conditions where the overall charge of NBs reversed to the negative value. Studies showed that surfactants adsorb at the surface of NBs such that polar heads orient towards the bubble through electrostatic forces and chains rearrange outwards by hydrophobic forces and lead to a change in the zeta potential of NBs, depending on the charge of their polar groups [179]. Similarly, Cho et al. [17] showed that the equilibrium state between partially ionized micelles and fully ionized monomers of surfactants can stabilize NBs.

Moreover, alkaline conditions may lead to the formation of finer and more stable NBs because highly negatively charged bubbles will repulse each other and prevent inter-bubble aggregation and coalescence, as reported by various researchers [20,195,196]. As mentioned earlier, the repulsion forces among NBs due to their negative surface charge can encourage bubble stability and decrease the rate of bubble coalescence. The zeta potentials of bubbles with different electrolytes, reported by numerous authors, show similarities, and their results are reviewed elsewhere [197]. For example, Uchida et al. [198] showed that a solution containing 100 mM NaCl can improve the stability of O_2 NBs for over a week; however, an excess concentration over an optimal amount may shorten the durability of NBs and accelerate the rate of coalescence. The stabilizing effect of surface charge can also be attributed to the relative arrangement of the water structure at the air/water interface. Bui et al. [117] performed a detailed study on the effect of different chemicals on the average size and zeta potential of NBs. They showed that bubbles in the presence of EDTA (ethylenediaminetetraacetic acid), glucose, and Na^+ remained nano-sized because of the lower adsorption of possible species at the bubble surface, whereas bubbles in DODAB (dimethyldioctadecylammonium bromide) and trivalent metal ions became submicron-sized after 90 min. The stability of NBs in the presence of Na^+ was in agreement with results reported elsewhere [198]. EDTA, glucose, and Na^+ gave a negative surface charge to NBs, whereas DODAB, Al^{3+}, and Fe^{3+} provided NBs with negatively charged surfaces. Interestingly in all solutions, the zeta potential of NBs declined as the solution pH increased from 2 to 12. Based on the works by Bui et al. [117], the possible mechanism for the creation of negative charge at the surface of NBs can be attributed mainly to OH^- (from EDTA) and the total charge of the inner surface and adsorption layer, or to a lesser extent, to Na^+ added to the solution due to the balance between inner surface charges and those of Na^+ adsorbed at the air/water interface. Moreover, the positive charge at the surface of NBs can be attributed to the partial balance between the negatively charged inner NBs surface and cations (R^+) adsorbed (from trivalent metal ions or the cationic surfactants) at the air/water interface. Generally, the NBs zeta potential may shift positively, provided the sum of the adsorbed cations' positive charges is greater than the sum of negative charges on the inner surface.

Hewage et al. [197] investigated the effect of ionic strength of electrolyte solutions on the stability of NBs. They examined various electrolytes including NaCl, Na_2SO_4, Na_3PO_4, $CaCl_2$, and $FeCl_3$, and concluded that compared to the bulk liquid, cations have higher concentrations at the surface of NBs. They also demonstrated that the adsorption of low-valence cations provides a negative charge at the surface of NBs under neutral-to-alkaline pH.

5. NB-Assisted Flotation

Traditionally used mechanical flotation cells dramatically decrease the recoverability of ultrafine and coarse particles in the presence of CBs due to the low probability of particle–bubble collision and high efficiency of detachment [34,64,187,188,199]. Studies have proven that creating small bubbles can successfully increase the flotation recovery of different mineral types (Figure 10). Improved flotation recoveries have been obtained for both ultrafine (<10–20 µm) and coarse (>200 µm) particles [11–13,24,64,106,132,133,200]. Most

attempts have been performed on mono-minerals, and mostly quartz, while little attention has been given to bulk samples. For instance, Zhou et al. [5] investigated the effect of hydrodynamic cavitation on fine silica recovery, which increased in the presence of ultrafine bubbles from 30 to 53% at a low flow velocity of 15 m/s. Nazari et al. [34] obtained an elevation of 21% for coarse quartz particles ($-425 + 106$ μm). For the same type of mineral, Rosa and Rubio [63] attained a significant increase (from 52 to 75%) in quartz ($d_{50} = 290$ μm) recovery in the presence of ultrafine bubbles. Following this, Calgaroto et al. [61] found that the injection of NBs (200–720 nm) along with CBs (400–800 μm) improved flotation recoveries of fine- and ultrafine-sized quartz particles. According to the results, flotation with single NBs was not effective due to their very low lifting power and poor buoyancy.
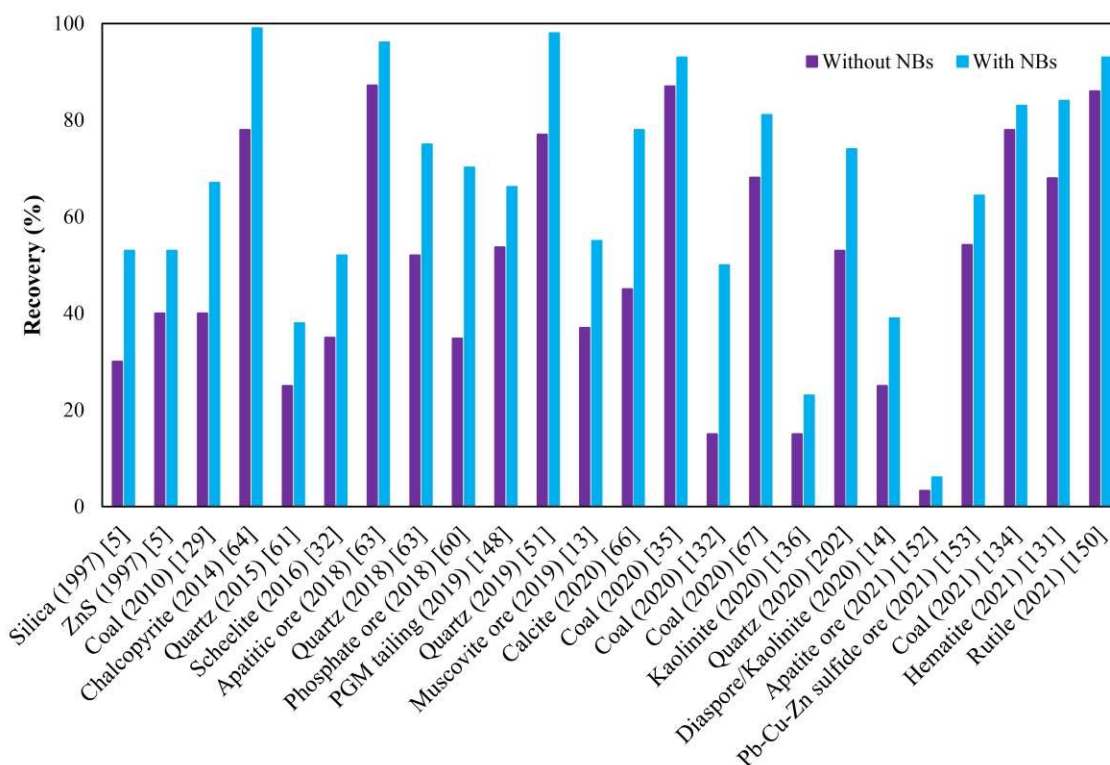
Figure 10. Studies conducted on NBs-assisted flotation in mechanically agitated flotation cells in 1997–2021 [5,13,14,32,35,51,60,61,63,64,66,67,129,131–136,148,150,152–154,201,202].

In addition to quartz, several studies have reported a similar trend for metallic and non-metallic minerals. A study showed an increase of 13% in the recovery of ZnS particles compared to flotation with CBs [5]. Ahmadi et al. [64] confirmed that the flotation recovery of fine ($-38 + 14$ μm) and ultrafine ($-14 + 5$ μm) chalcopyrite particles with NBs increased by approximately 16–21%. Such enhancement was linked to the improved probability of particle–bubble attachment. Additionally, collector and frother consumption were decreased by 50% and 75%, respectively. An improvement of 30% was reported for fine P_2O_5 particles [63]. The presence of NBs increased the flotation recovery of coal particles by approximately more than 35% [134]. NBs also played a crucial role in the entrainment of kaolinite particles in flotation [136]. Zhou et al. [14] found that NBs could efficiently remove the sodium oleate (NaOl) from diaspore surfaces. Li et al. [67] proposed that in the presence of NBs and polyaluminum chloride, the final combustible recovery of coal particles increased by about 13%.

Some studies have shown that the NBs produced by hydrodynamic cavitation can improve the flotation performance of fine and coarse particles as well as decrease the consumption of reagents [5,109,182,202]. They concluded that the hydrophobic bridging effect of NBs can promote flotation of fine particles. For example, Zhou et al. [32] found that ultrafine bubbles can improve ultrafine scheelite particles' aggregation and their recovery

to ca. 17% when the concentration of NaOl was low. The adsorption behavior of bulk NBs produced using hydrodynamic cavitation on the muscovite surface in the presence of dodecylamine (DDA) was investigated by Zhou et al. [13]. They reported that ultrafine bubbles adsorb on the muscovite surface in the presence of DDA, changing its surfaces to more hydrophobic and finally increasing the flotation performance by approximately 18%. However, this study did not discuss the interaction between generated bubbles and the collector or the adsorption behavior of bubbles on the muscovite surface. Seemingly, the NBs are surface-modified with a collector and can provide selective adsorption of the ionic active sites exposed to the mineral surface.

Tao et al. [133] studied the influence of ultrafine bubbles on reverse anionic flotation of hematite particles. NBs significantly increased the Fe recovery (approximately 16%) at all varying reagent dosages. They found that starch dosage had an important effect on the concentrate Fe grade and recovery in reverse hematite flotation.

In addition to the mechanical flotation cells, column flotation experiments performed by some researchers have demonstrated the effectiveness of NB-assisted flotation technology mostly on coal and phosphate particles. Figure 11 displays most of these works. For example, it was shown that ultrafine bubbles increased P_2O_5 and coal flotation recoveries by 10–30% and 8–27%, respectively, at different particle size fractions [24,131]. Li et al. [203] conducted the flotation of siliceous phosphate ore using NBs, but no specific information was reported on the bubble size. Xiong et al. [55] reported such tendencies (about 14%) in the presence of NBs for P_2O_5 particles.
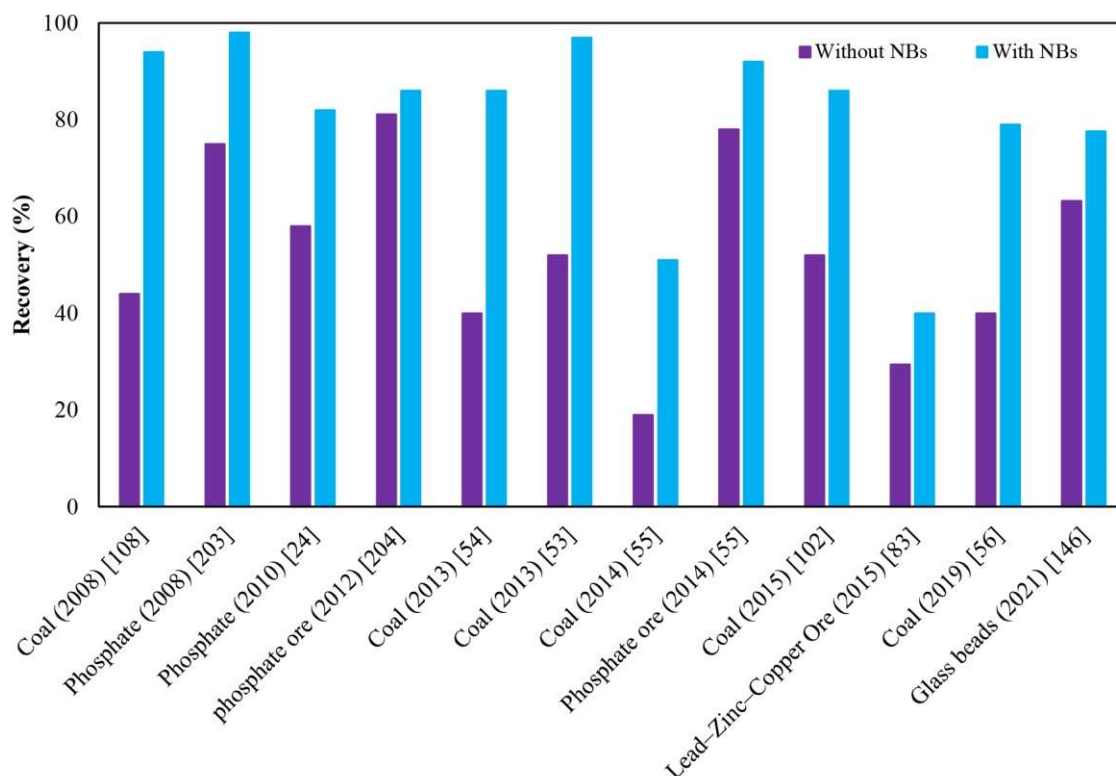
Figure 11. Studies about NBs-assisted flotation in column flotation cells, 2008–2021 [24,53–56,83,101,102,107,108,146,202–204].

NBs were formed by a self-aerating bubble generator in a cyclone flotation column. Recovery of fine particles (<10 μm) reached 86%, which was increased by 5% compared with that of direct flow circulation [203]. In another work, Sobhy and Tao [53] investigated the recovery of coal particles in a column flotation in the presence/absence of NBs, where the bubbles were formed through dissolved air (DAF) in coal slurry. Results showed an enhancement of about 50% (from 47 to 97%) in the combustible recovery of −150 μm coal

particles. Fan et al. [54] indicated that in coal particles with coarse sizes of $-355 + 600$ μm, the recovery was enhanced from 13 to 22% using NBs, while the corresponding improvements were 8%, 28%, and 46% in fine particles of $-38 + 45$, $-20 + 38$, and -20 μm, respectively. Experimental results reported by Ma et al. [56] showed that coal recovery in the presence of ultrafine bubbles increased by 10–39%, halved frother and collector dosages, reduced the required air consumption, and increased the capacity of the flotation column to some degree.

Table 4 presents the scale and the level of recovery improvement of coal and mineral flotation assisted with NBs. Considering the results given in the cases studies, it was recognized that the most attention was paid to proving an improvement in recovering only some typical minerals and coal particles in the presence of ultrafine bubbles. Almost all of them were performed under different experimental setups, reagent regimes, and operating conditions, leading to the creation of slight differences among the results. Thus, the role of NBs on the grade and selective separation was relatively overlooked and still needs to be understood and explained. Another challenge in these studies is rescaling the laboratory results to industrial applications. As can be seen in Table 4, efforts in the industrial use of NBs are very limited and constrained to coal flotation on a semi-industrial scale. The reason for this comes from the simplicity of the coal flotation process compared to complex ores such as sulfides. Therefore, the development of investigations in the field of exploration of mechanisms and the interaction of NBs with particles in complex systems (no single-mineral system) will be the first step to find industrialization solutions for the application of NBs in the mineral processing industry. Additionally, according to Table 4, the method used on the largest scale is of cavitation type. This method is currently used on a large scale in spargers used in flotation columns. For this reason, the efficiency of this method has been evaluated and approved on an industrial scale. Therefore, it seems that the main challenge in large-scale applications of NBs does not arise from mechanical aspects.

Flotation kinetics include several sub-processes that take place in the pulp and froth phases, including particle–bubble collision and attachment, transport of the particle–bubble aggregate to the froth phase, and recovery of the particle from the froth phase to a concentrate launder. The bubble size and froth stability significantly affect these sub-processes [204]. The flotation rate constant depends on the particle hydrophobicity, particle size, solids content, feed rate, froth depth, reagent type, reagent dosage, gas flow rate, and bubble diameter (bubble generators) [205].

Two factors that contribute to the increased flotation rate constant are (i) NBs formed on hydrophobic particles may cause agglomeration by a bubble-bridging mechanism resulting in an enhancement of the collision efficiency; and (ii) particles frosted with the bubbles may present a surface favorable to attachment to CBs. In this regard, several case studies addressed an improvement in the flotation kinetics rate (k) of minerals in the presence of NBs (Table 5). For instance, Nazari et al. [51] showed that k of quartz coarse particles improved by 21% in the presence of DDA-NBs. Han et al. [35] reported an endearment of 37% in coal flotation kinetics, attributing it to an increase in collision and attachment probabilities and a reduction in detachment probability. In another work, the flotation kinetics rate of hematite was reduced from 3 to less than 1 min [133]. Farrokhpay et al. [201] focused on the kinetics of fine particles in the presence of MBs and CBs, reporting higher values when the NBs were applied. One main reason for higher kinetic rates in the presence of ultrafine bubbles is related to the increased hydrophobicity expressed by the water contact angle. For instance, the water contact angle on quartz measured by the sessile drop technique increased from 18° (standard deviation = 3.6°) to 46° (standard deviation = 7°) in the presence of NBs [61].

Table 4. Summary of observed change in the flotation recovery for mechanical and column flotation cases. UN: unknown or not mentioned in the manuscript.

Flotation Cell	Materials	Scale	NBs Size (nm)	Equipment	Relative Change (%)	Refs.
Mechanical flotation	Silica	Laboratory	UN	Venturi tube	23	[5]
	ZnS	Laboratory	UN	Venturi tube	13	[5]
	Quartz	Laboratory	171	Venturi tube	21	[34]
	Quartz	Laboratory	150–200	Depressurization of DI water	23	[63]
	Quartz	Laboratory	200–720	Steel needle valve	13	[61]
	Chalcopyrite	Laboratory	358	Venturi tube	21	[64]
	P_2O_5	Laboratory	150–200	Depressurization of DI water	30	[63]
	Coal	Laboratory	~300	Hydrodynamic cavitation	35	[134]
	Kaolinite	Laboratory	<120	Decompression	8	[136]
	Diaspore/kaolinite	Laboratory	100–300	Venturi tube	14	[14]
	Coal	Laboratory	100–200	Ultrasonic cavitation	13	[67]
	Scheelite	Laboratory	UN	Venturi tube	17	[32]
	Muscovite	Laboratory	100	Venturi tube	18	[13]
	Hematite	Laboratory	150–280	Venturi tube	16	[133]
Column flotation	P_2O_5	Laboratory	<1 μm	Venturi tube	30	[24]
	Coal	Pilot	<1 μm	Venturi tube	27	[131]
	P_2O_5	Laboratory	150–240	Venturi tube	14	[55]
	Coal	Laboratory	<1 μm	Venturi tube	50	[53]
	Coal	Pilot	700	Hydrodynamic cavitation	46	[54]
	Coal	Laboratory	160–250	Venturi tube	39	[56]

Table 5. Summary of observed changes in the flotation rate constant for mechanical and column flotation cases.

Flotation Cell	Materials	Relative Change (%)	Refs.
Mechanical flotation	Silica	40	[5]
	Zns	65	[5]
	Coal	98.4	[131]
	PGM	61	[148]
	Quartz	36	[51]
	Muscovite	26	[13]
	Coal	33.6	[35]
	Quartz	75	[200]
	Apatite ore	10.4	[153]
	Coal	14.4	[135]
	Rutile	42.7	[150]
Column flotation	Coal	40	[97]
	Phosphate	109	[24]
	Coal	160	[54]

6. Conclusions and Future Works

Efficient recovery of fine, ultrafine, and coarse particles has been a long-standing challenge in flotation processes for over a century. A wide diversity of research investigations have been undertaken to overcome this, and recently, NB-assisted flotation has appeared as a promising technique. To this end, the present review addresses the key opportunities and challenges regarding the generation and detection of ultrafine bubbles as well as the effectiveness in recovering particles and flotation kinetics. The following findings were highlighted.

- Evaluating literature data showed that while CB analyzers are used to detect ultrafine bubble sizes and distributions, the most commonly used methods are LPSA and NTA instruments, which may include a reasonable amount of bias.
- Alkaline environments lead to the formation of smaller and stable bubbles because highly negatively charged bubbles tend to repel each other, which prevents inter-bubble aggregation and coalescence.
- Hydrodynamic cavitation was found to be the most popular technique for producing NBs, which can be likely extended to industrial applications in the future.
- An integrated separation of minerals in flotation using ultrafine bubbles reduces collector and frother consumption and improves not only recovery but also the flotation rate constant of fine, ultrafine, and coarse particles.
- Flotation in the presence of NBs can elevate the recoverability of mono-minerals by approximately 15% and 20% on average using mechanical and column flotation cells, respectively.
- Most of the focus in the last two decades has been on approving the existence, stability, and impact of single-mineral flotation, and little attention and few reports have been on bulk and actual ores.

Considering the above conclusions and given information in the literature, the following future works are recommended:

- There are no solid comparative results concerning generating and observing ultrafine bubbles using commonly used apparatus. Thus, such information can help in better quantitative judgment among common techniques.
- Although some basic principles about how to generate and apply NBs to flotation research and operations are known, challenges remain in quantifying and mathematically describing their role in flotation.
- Future research should be focused on understanding the stabilization mechanisms of bubbles generated by different methods, optimizing their size ranges for maximized

flotation recovery, minimizing wear and damage in industrial operations, and intensifying the role of in situ NB nucleation on particles in flotation.

- From an economic point of view, there is no information in the literature about total costs versus metallurgical beneficiations.
- Although a reasonable degree of recovery improvement has been widely reported in the literature, researchers have rarely reported the impact of NBs on grade, separation efficiency, and selectivity of separation. Thus, further studies are recommended in this sense.
- The synergy of chemical, physical, and hydrodynamic features for NB generation in an energy-efficient, technically effective, and user-friendly manner, with controlled sizes of generated bubbles, are also important goals in the future.

Conflicts of Interest: The authors declare no conflict of interest.

References

1. Nirmalkar, N.; Pacek, A.; Barigou, M. On the existence and stability of bulk nanobubbles. *Langmuir* **2018**, *34*, 10964–10973. [CrossRef]
2. Weijs, J.H.; Seddon, J.R.; Lohse, D. Diffusive shielding stabilizes bulk nanobubble clusters. *ChemPhysChem* **2012**, *13*, 2197–2204. [CrossRef]
3. Fox, F.E.; Herzfeld, K.F. Gas bubbles with organic skin as cavitation nuclei. *J. Acoust. Soc. Am.* **1954**, *26*, 984–989. [CrossRef]
4. Zhou, Z.A.; Xu, Z.; Finch, J.A. On the role of cavitation in particle collection during flotation—A critical review. *Miner. Eng.* **1994**, *7*, 1073–1084. [CrossRef]
5. Zhou, Z.; Xu, Z.; Finch, J.; Hu, H.; Rao, S. Role of hydrodynamic cavitation in fine particle flotation. *Int. J. Miner. Process.* **1997**, *51*, 139–149. [CrossRef]
6. Zhou, Z.A.; Xu, Z.; Finch, J.A.; Masliyah, J.H.; Chow, R.S. On the role of cavitation in particle collection in flotation—A critical review. II. *Miner. Eng.* **2009**, *22*, 419–433. [CrossRef]
7. Lou, S.T.; Ouyang, Z.Q.; Zhang, Y.; Li, X.J.; Hu, J.; Li, M.Q.; Yang, F.J. Nanobubbles on solid surface imaged by atomic force microscopy. *J. Vac. Sci. Technol. B Microelectron. Nanometer Struct. Process. Meas. Phenom.* **2000**, *18*, 2573–2575. [CrossRef]
8. Zatzkis, H. Sound field of a moving cylinder and a moving sphere. *J. Acoust. Soc. Am.* **1954**, *26*, 169–173. [CrossRef]
9. Eklund, F.; Swenson, J. Stable Air Nanobubbles in Water: The Importance of Organic Contaminants. *Langmuir* **2018**, *34*, 11003–11009. [CrossRef]
10. Li, D.; Jing, D.; Pan, Y.; Bhushan, B.; Zhao, X. Study of the relationship between boundary slip and nanobubbles on a smooth hydrophobic surface. *Langmuir* **2016**, *32*, 11287–11294. [CrossRef]
11. Fan, F.; Daniel, T.; Honaker, R.; Zhenfu, L. Nanobubble generation and its applications in froth flotation (part II): Fundamental study and theoretical analysis. *Min. Sci. Technol. (China)* **2010**, *20*, 159–177. [CrossRef]
12. Nazari, S.; Shafaei, S.Z.; Shahbazi, B.; Chelgani, S.C. Study relationships between flotation variables and recovery of coarse particles in the absence and presence of nanobubble. *Colloids Surf. A Physicochem. Eng. Asp.* **2018**, *559*, 284–288. [CrossRef]
13. Zhou, W.; Niu, J.; Xiao, W.; Ou, L. Adsorption of bulk nanobubbles on the chemically surface-modified muscovite minerals. *Ultrason. Sonochemistry* **2019**, *51*, 31–39. [CrossRef] [PubMed]
14. Zhou, W.; Liu, K.; Wang, L.; Zhou, B.; Niu, J.; Ou, L. The role of bulk micro-nanobubbles in reagent desorption and potential implication in flotation separation of highly hydrophobized minerals. *Ultrason. Sonochemistry* **2020**, *64*, 104996. [CrossRef]
15. Lu, X.M.; Yuan, B.; Zhang, X.R.; Yang, K.; Ma, Y.Q. Molecular modeling of transmembrane delivery of paclitaxel by shock waves with nanobubbles. *Appl. Phys. Lett.* **2017**, *110*, 023701. [CrossRef]
16. Temesgen, T.; Bui, T.T.; Han, M.; Kim, T.I.; Park, H. Micro and nanobubble technologies as a new horizon for water-treatment techniques: A review. *Adv. Colloid Interface Sci.* **2017**, *246*, 40–51. [CrossRef]
17. Cho, S.H.; Kim, J.Y.; Chun, J.H.; Kim, J.D. Ultrasonic formation of nanobubbles and their zeta-potentials in aqueous electrolyte and surfactant solutions. *Colloids Surf. A Physicochem. Eng. Asp.* **2005**, *269*, 28–34. [CrossRef]
18. Najafi, A.S.; Drelich, J.; Yeung, A.; Xu, Z.; Masliyah, J. A novel method of measuring electrophoretic mobility of gas bubbles. *J. Colloid Interface Sci.* **2007**, *308*, 344–350. [CrossRef]
19. Bhondayi, C. Flotation froth phase bubble size measurement. *Miner. Process. Extr. Metall. Rev.* **2022**, *43*, 251–273. [CrossRef]

20. Bournival, G.; Ata, S.; Jameson, G.J. Bubble and froth stabilizing agents in froth flotation. *Miner. Process. Extr. Metall. Rev.* **2017**, *38*, 366–387. [CrossRef]

21. Azevedo, A.; Oliveira, H.; Rubio, J. Bulk nanobubbles in the mineral and environmental areas: Updating research and applications. *Adv. Colloid Interface Sci.* **2019**, *271*, 101992. [CrossRef]

22. Yang, S.; Dammer, S.M.; Bremond, N.; Zandvliet, H.J.; Kooij, E.S.; Lohse, D. Characterization of nanobubbles on hydrophobic surfaces in water. *Langmuir* **2007**, *23*, 7072–7077. [CrossRef] [PubMed]

23. Ushikubo, F.Y.; Furukawa, T.; Nakagawa, R.; Enari, M.; Makino, Y.; Kawagoe, Y.; Shiina, T.; Oshita, S. Evidence of the existence and the stability of nano-bubbles in water. *Colloids Surf. A Physicochem. Eng. Asp.* **2010**, *361*, 31–37. [CrossRef]

24. Fan, F.; Daniel, T.; Honaker, R.; Zhenfu, L. Nanobubble generation and its applications in froth flotation (part III): Specially designed laboratory scale column flotation of phosphate. *Min. Sci. Technol. (China)* **2010**, *20*, 317–338. [CrossRef]

25. Tuziuti, T.; Yasui, K.; Kanematsu, W. Influence of addition of degassed water on bulk nanobubbles. *Ultrason. Sonochemistry* **2018**, *43*, 272–274. [CrossRef]

26. Nazari, S.; Hassanzadeh, A. The effect of reagent type on generating bulk sub-micron (nano) bubbles and flotation kinetics of coarse-sized quartz particles. *Powder Technol.* **2020**, *374*, 160–171. [CrossRef]

27. Svetovoy, V.B. Spontaneous chemical reactions between hydrogen and oxygen in nanobubbles. *Curr. Opin. Colloid Interface Sci.* **2021**, *52*, 101423. [CrossRef]

28. Yasuda, K.; Matsushima, H.; Asakura, Y. Generation and reduction of bulk nanobubbles by ultrasonic irradiation. *Chem. Eng. Sci.* **2019**, *195*, 455–461. [CrossRef]

29. Kikuchi, K.; Nagata, S.; Tanaka, Y.; Saihara, Y.; Ogumi, Z. Characteristics of hydrogen nanobubbles in solutions obtained with water electrolysis. *J. Electroanal. Chem.* **2007**, *600*, 303–310. [CrossRef]

30. Aldrich, C.; Feng, D. The effect of mothers on bubble size distributions in flotation pulp phases and surface froths. *Miner. Eng.* **2000**, *13*, 1049–1057. [CrossRef]

31. Gogate, P.R.; Pandit, A.B. Hydrodynamic cavitation reactors: A state of the art review. *Rev. Chem. Eng.* **2001**, *17*, 1–85. [CrossRef]

32. Zhou, W.; Chen, H.; Ou, L.; Shi, Q. Aggregation of ultra-fine scheelite particles induced by hydrodynamic cavitation. *Int. J. Miner. Process.* **2016**, *157*, 236–240. [CrossRef]

33. Oliveira, H.; Azevedo, A.; Rubio, J. Nanobubbles generation in a high-rate hydrodynamic cavitation tube. *Miner. Eng.* **2018**, *116*, 32–34. [CrossRef]

34. Nazari, S.; Chelgani, S.C.; Shafaei, S.; Shahbazi, B.; Matin, S.; Gharabaghi, M. Flotation of coarse particles by hydrodynamic cavitation generated in the presence of conventional reagents. *Sep. Purif. Technol.* **2019**, *220*, 61–68. [CrossRef]

35. Han, H.; Liu, A.; Wang, H. Effect of hydrodynamic cavitation assistance on different stages of coal flotation. *Minerals* **2020**, *10*, 221. [CrossRef]

36. Rowe, P.N.; Matsuno, R. Single bubbles injected into a gas fluidised bed and observed by X-rays. *Chem. Eng. Sci.* **1971**, *26*, 923–935. [CrossRef]

37. Hoang, D.H.; Hassanzadeh, A.; Peuker, U.A.; Rudolph, M. Impact of flotation hydrodynamics on the optimization of fine-grained carbonaceous sedimentary apatite ore beneficiation. *Powder Technol.* **2019**, *345*, 223–233. [CrossRef]

38. Sung, J.S.; Burgess, J.M. A laser-based method for bubble parameter measurement in two-dimensional fluidised beds. *Powder Technol.* **1987**, *49*, 165–175. [CrossRef]

39. Naosuke, O.; Koizumi, Y.; Kamide, H.; Ohno, S.; Ito, K. Effect of physical properties on gas entrainment rate from free surface by vortex. *Int. Conf. Nucl. Eng.* **2013**, *55836*, V006T16A029.

40. Rodrigues, R.T.; Rubio, J. New basis for measuring the size distribution of bubbles. *Miner. Eng.* **2003**, *16*, 757–765. [CrossRef]

41. Zhou, Z.A.; Egiebor, N.O.; Plitt, L.R. Frother effects on bubble size estimation in a flotation column. *Miner. Eng.* **1993**, *6*, 55–67. [CrossRef]

42. Zhang, X.Y.; Wang, Q.S.; Wu, Z.X.; Tao, D.P. An experimental study on size distribution and zeta potential of bulk cavitation nanobubbles. *Int. J. Miner. Metall. Mater.* **2020**, *27*, 152–161. [CrossRef]

43. Zhang, X.; Liu, X.; Zhong, Y.; Zhou, Z.; Huang, Y.; Sun, C.Q. Nanobubble skin supersolidity. *Langmuir* **2016**, *32*, 11321–11327. [CrossRef] [PubMed]

44. Sun, Y.; Xie, G.; Peng, Y.; Xia, W.; Sha, J. Stability theories of nanobubbles at solid–liquid interface: A review. *Colloids Surf. A Physicochem. Eng. Asp.* **2016**, *495*, 176–186. [CrossRef]

45. Zhou, S.; Wang, X.; Bu, X.; Wang, M.; An, B.; Shao, H.; Ni, C.; Peng, Y.; Xie, G. A novel flotation technique combining carrier flotation and cavitation bubbles to enhance separation efficiency of ultra-fine particles. *Ultrason. Sonochemistry* **2020**, *64*, 105005. [CrossRef]

46. Wu, C.; Nesset, K.; Masliyah, J.; Xu, Z. Generation and characterization of submicron size bubbles. *Adv. Colloid Interface Sci.* **2012**, *179*, 123–132. [CrossRef]

47. Tussupbayev, N.K.; Rulyov, N.N.; Kravtchenco, O.V. Microbubble augmented flotation of ultrafine chalcopyrite from quartz mixtures. *Miner. Process. Extr. Metall.* **2016**, *125*, 5–9. [CrossRef]

48. Tao, D.; Sobhy, A. Nanobubble effects on hydrodynamic interactions between particles and bubbles. *Powder Technol.* **2019**, *346*, 385–395. [CrossRef]

49. Knüpfer, P.; Ditscherlein, L.; Peuker, U.A. Nanobubble enhanced agglomeration of hydrophobic powders. *Colloids Surf. A Physicochem. Eng. Asp.* **2017**, *530*, 117–123. [CrossRef]

50. Nazari, S.; Shafaei, S.Z.; Hassanzadeh, A.; Azizi, A.; Gharabaghi, M.; Ahmadi, R.; Shahbazi, B. Study of effective parameters on generating submicron (nano)-bubbles using the hydrodynamic cavitation. *Physicochem. Probl. Miner. Process.* **2020**, *56*, 884–904. [CrossRef]

51. Nazari, S.; Shafaei, S.Z.; Gharabaghi, M.; Ahmadi, R.; Shahbazi, B.; Fan, M. Effects of nanobubble and hydrodynamic parameters on coarse quartz flotation. *Int. J. Min. Sci. Technol.* **2019**, *29*, 289–295. [CrossRef]

52. Weber, M.E.; Paddock, D. Interceptional and gravitational collision efficiencies for single collectors at intermediate Reynolds numbers. *J. Colloid Interface Sci.* **1983**, *94*, 328–335. [CrossRef]

53. Sobhy, A.; Tao, D. Nanobubble column flotation of fine coal particles and associated fundamentals. *Int. J. Miner. Process.* **2013**, *124*, 109–116. [CrossRef]

54. Fan, M.; Tao, D.; Zhao, Y.; Honaker, R. Effect of nanobubbles on the flotation of different sizes of coal particle. *Min. Metall. Explor.* **2013**, *30*, 157–161. [CrossRef]

55. Xiong, Y. Bubble Size Effects in Coal Flotation and Phosphate Reverse Flotation Using a Pico-Nano Bubble Generator. Ph.D. Thesis, West Virginia University, Morgantown, VA, USA, 2014.

56. Ma, F.; Tao, D.; Tao, Y. Effects of nanobubbles in column flotation of Chinese sub-bituminous coal. *Int. J. Coal Prep. Util.* **2019**, 1–17. [CrossRef]

57. Liu, Y.; Tao, X.; Jiang, H.; Chen, R. Intensification of fine apatite flotation with microbubble generation and inclined plates in the flotation column. *Chem. Eng. Process. Process Intensif.* **2020**, *157*, 108133. [CrossRef]

58. Kruszelnicki, M.; Hassanzadeh, A.; Legawiec, K.J.; Polowczyk, I.; Kowalczuk, P.B. Effect of ultrasound pre-treatment on carbonaceous copper-bearing shale flotation. *Ultrason. Sonochemistry* **2022**, *84*, 105962. [CrossRef] [PubMed]

59. Tao, D.; Fan, M.; Honaker, R.; Parekh, B.K. Picobubble enhanced flotation of coarse phosphate particles. In Proceedings of the 23th International Mineral Processing Congress, Istanbul, Turkey, 3–8 September 2006.

60. Pourkarimi, Z.; Rezai, B.; Noaparast, M. Nanobubbles effect on the mechanical flotation of phosphate ore fine particles. *Physicochem. Probl. Miner. Process.* **2018**, *54*, 278–292.

61. Calgaroto, S.; Azevedo, A.; Rubio, J. Flotation of quartz particles assisted by nanobubbles. *Int. J. Miner. Process.* **2015**, *137*, 64–70. [CrossRef]

62. Nazari, S.; Shafaei, S.Z.; Gharabaghi, M.; Ahmadi, R.; Shahbazi, B. Effect of frother type and operational parameters on nano bubble flotation of quartz coarse particles. *J. Min. Environ.* **2018**, *9*, 539–546.

63. Rosa, A.; Rubio, J. On the role of nanobubbles in particle-bubble adhesion for the flotation of quartz and apatitic minerals. *Miner. Eng.* **2018**, *127*, 178–184. [CrossRef]

64. Ahmadi, R.; Khodadadi, D.A.; Abdollahy, M.; Fan, M. Nano-microbubble flotation of fine and ultrafine chalcopyrite particles. *Int. J. Min. Sci. Technol.* **2014**, *24*, 559–566. [CrossRef]

65. Khan, P.; Zhu, W.; Huang, F.; Gao, W.; Khan, N.A. Micro- nanobubble technology and water-related application. *Water Supply* **2020**, *20*, 2021–2035. [CrossRef]

66. Wang, Y.; Pan, Z.; Jiao, F.; Qin, W. Understanding bubble growth process under decompression and its effects on the flotation phenomena. *Miner. Eng.* **2020**, *145*, 106066. [CrossRef]

67. Li, C.; Xu, M.; Zhang, H. Efficient separation of high-ash fine coal by the collaboration of nanobubbles and polyaluminum chloride. *Fuel* **2020**, *260*, 116325. [CrossRef]

68. Lohse, D.; Zhang, X. Surface nanobubbles and nanodroplets. *Rev. Mod. Phys.* **2015**, *87*, 981. [CrossRef]

69. Kim, S.; Kim, H.; Han, M.; Kim, T. Generation of sub-micron (nano) bubbles and characterization of their fundamental properties. *Environ. Eng. Res.* **2019**, *24*, 382–388. [CrossRef]

70. Kim, J.Y.; Song, M.G.; Kim, J.D. Zeta potential of nanobubbles generated by ultrasonication in aqueous alkyl polyglycoside solutions. *J. Colloid Interface Sci.* **2000**, *223*, 285–291. [CrossRef]

71. Oeffinger, B.E.; Wheatley, M.A. Development and characterization of a nano-scale contrast agent. *Ultrasonics* **2004**, *42*, 343–347. [CrossRef]

72. Ohgaki, K.; Khanh, N.Q.; Joden, Y.; Tsuji, A.; Nakagawa, T. Physicochemical approach to nanobubble solutions. *Chem. Eng. Sci.* **2010**, *65*, 1296–1300. [CrossRef]

73. Etchepare, R.; Oliveira, H.; Nicknig, M.; Azevedo, A.; Rubio, J. Nanobubbles: Generation using a multiphase pump, properties and features in flotation. *Miner. Eng.* **2017**, *112*, 19–26. [CrossRef]

74. Michailidi, E.D.; Bomis, G.; Varoutoglou, A.; Kyzas, G.Z.; Mitrikas, G.; Mitropoulos, A.C.; Efthimiadou, E.K.; Favvas, E.P. Bulk nanobubbles: Production and investigation of their formation/stability mechanism. *J. Colloid Interface Sci.* **2020**, *564*, 371–380. [CrossRef] [PubMed]

75. Zhang, F.; Sun, L.; Yang, H.; Gui, X.; Schönherr, H.; Kappl, M.; Cao, Y.; Xing, Y. Recent advances for understanding the role of nanobubbles in particles flotation. *Adv. Colloid Interface Sci.* **2021**, *291*, 102403. [CrossRef] [PubMed]

76. Alheshibri, M.; Baroot, A.; Shui, L.; Zhang, M. Nanobubbles and nanoparticles. *Curr. Opin. Colloid Interface Sci.* **2021**, *55*, 101470. [CrossRef]

77. Li, C.; Zhang, H. Surface nanobubbles and their roles in flotation of fine particles—A review. *J. Ind. Eng. Chem.* **2022**, *106*, 37–51. [CrossRef]

78. Li, C.; Zhang, H. A review of bulk nanobubbles and their roles in flotation of fine particles. *Powder Technol.* **2022**, *395*, 618–633. [CrossRef]

79. Yasui, K.; Tuziuti, T.; Kanematsu, W. Mysteries of bulk nanobubbles (ultrafine bubbles); stability and radical formation. *Ultrason. Sonochemistry* **2018**, *48*, 259–266. [CrossRef]

80. Leroy, V.; Norisuye, T. Investigating the existence of bulk nanobubbles with ultrasound. *ChemPhysChem* **2016**, *17*, 2787–2790. [CrossRef]

81. Bu, X.; Alheshibri, M. The effect of ultrasound on bulk and surface nanobubbles: A review of the current status. *Ultrason. Sonochemistry* **2021**, *76*, 105629. [CrossRef]

82. Chen, Y.; Truong, V.N.T.; Bu, X.; Xie, G. A review of effects and applications of ultrasound in mineral flotation. *Ultrason. Sonochemistry* **2020**, *60*, 104739. [CrossRef]

83. Kursun, H.; Ulusoy, U. Zinc recovery from a lead-zinc-copper ore by ultrasonically assisted column flotation. *Part. Sci. Technol.* **2015**, *33*, 349–356. [CrossRef]

84. Zimmerman, W.B.; Tesar, V.; Bandulasena, H.H. Towards energy efficient nanobubble generation with fluidic oscillation. *Curr. Opin. Colloid Interface Sci.* **2011**, *16*, 350–356. [CrossRef]

85. Miastkowska, M.A.; Banach, M.; Pulit-Prociak, J.; Sikora, E.S.; Głogowska, A.; Zielina, M. Statistical analysis of optimal ultrasound emulsification parameters in thistle-oil nanoemulsions. *J. Surfactants Deterg.* **2017**, *20*, 233–246. [CrossRef] [PubMed]

86. Xiao, W.; Zhao, Y.; Yang, J.; Ren, Y.; Yang, W.; Huang, X.; Zhang, L. Effect of sodium oleate on the adsorption morphology and mechanism of nanobubbles on the mica surface. *Langmuir* **2019**, *35*, 9239–9245. [CrossRef]

87. Chen, Y.; Bu, X.; Truong, V.N.T.; Peng, Y.; Xie, G. Study on the effects of pre-conditioning time on the floatability of molybdenite from the perspective of cavitation threshold. *Miner. Eng.* **2019**, *141*, 105845. [CrossRef]

88. Hassanzadeh, A.; Sajjady, S.A.; Gholami, H.; Amini, S.; Özkan, S.G. An improvement on selective separation by applying ultrasound to rougher and re-cleaner stages of copper flotation. *Minerals* **2020**, *10*, 619. [CrossRef]

89. Hassanzadeh, A.; Gholami, H.; Özkan, S.G.; Niedoba, T.; Surowiak, A. Effect of power ultrasound on wettability and collector-less floatability of chalcopyrite, pyrite and quartz. *Minerals* **2021**, *11*, 48. [CrossRef]

90. Jin, F.; Ye, J.; Hong, L.; Lam, H.; Wu, C. Slow relaxation mode in mixtures of water and organic molecules: Supramolecular structures or nanobubbles? *J. Phys. Chem. B* **2007**, *111*, 2255–2261. [CrossRef]

91. Xiao, Q.; Liu, Y.; Guo, Z.; Liu, Z.; Lohse, D.; Zhang, X. Solvent exchange leading to nanobubble nucleation: A molecular dynamics study. *Langmuir* **2017**, *33*, 8090–8096. [CrossRef]

92. Lou, S.; Gao, J.; Xiao, X.; Li, X.; Li, G.; Zhang, Y.; Li, M.; Sun, J.; Li, X.; Hu, J. Studies of nanobubbles produced at liquid/solid interfaces. *Mater. Charact.* **2002**, *48*, 211–214. [CrossRef]

93. Zhou, L.M.; Wang, S.; Qiu, J.; Wang, L.; Wang, X.Y.; Li, B.; Zhang, L.J.; Hu, J. Interfacial nanobubbles produced by long-time preserved cold water. *Chin. Phys. B* **2017**, *26*, 106803. [CrossRef]

94. Zhou, W.; Wu, C.; Lv, H.; Zhao, B.; Liu, K.; Ou, L. Nanobubbles heterogeneous nucleation induced by temperature rise and its influence on minerals flotation. *Appl. Surf. Sci.* **2020**, *508*, 145282. [CrossRef]

95. Zhang, X.H.; Zhang, X.D.; Lou, S.T.; Zhang, Z.X.; Sun, J.L.; Hu, J. Degassing and temperature effects on the formation of nanobubbles at the mica/water interface. *Langmuir* **2004**, *20*, 3813–3815. [CrossRef]

96. Tao, D. Role of bubble size in flotation of coarse and fine particles—A review. *Sep. Sci. Technol.* **2005**, *39*, 741–760. [CrossRef]

97. Fan, F.; Daniel, T.; Honaker, R.; Zhenfu, L. Nanobubble generation and its application in froth flotation (part I): Nanobubble generation and its effects on properties of microbubble and millimeter scale bubble solutions. *Min. Sci. Technol. (China)* **2010**, *20*, 1–19. [CrossRef]

98. Thornycroft, J.I.; Barnaby, S.W. Torpedo-boat destroyers. In *Minutes of the Proceedings of the Institution of Civil Engineers*; Thomas Telford-ICE Virtual Library: London, UK, 1895; Volume 122, pp. 51–69.

99. Pease, D.C.; Blinks, L.R. Cavitation from solid surfaces in the absence of gas nuclei. *J. Phys. Colloid Chem.* **1947**, *51*, 556–567. [CrossRef] [PubMed]

100. Sayed, A.A.S. Cavitation Nanobubble Enhanced Flotation Process for More Efficient Coal Recovery. Ph.D. Thesis, University of Kentucky, Lexington, KY, USA, 2013.

101. Xiong, Y.; Peng, F. Optimization of cavitation venturi tube design for pico and nano bubbles generation. *Int. J. Min. Sci. Technol.* **2015**, *25*, 523–529. [CrossRef]

102. Favvas, E.P.; Kyzas, G.Z.; Efthimiadou, E.K.; Mitropoulos, A.C. Bulk nanobubbles, generation methods and potential applications. *Curr. Opin. Colloid Interface Sci.* **2021**, *54*, 101455. [CrossRef]

103. Pourkarimi, Z.; Rezai, B.; Noaparast, N. Effective parameters on generation of nanobubbles by cavitation method for froth flotation applications. *Physicochem. Probl. Miner. Process.* **2017**, *53*, 920–942.

104. Wasmund, E.B. Flotation technology for coarse and fine particle recovery. In Proceedings of the Congreso Internacional De Flotacion De Minerales, Lima, Peru, 22 September 2014.

105. Hart, G.; Morgan, S.; Bramall, N.; Nicol, S. Enhanced Coal Flotation Using Picobubbles, Australia, 2002, CSIRO Report-C9048. Available online: https://www.acarp.com.au/reportcategory.aspx?catId=3&subCatId=25 (accessed on 10 January 2022).

106. Zhou, W.; Ou, L.; Shi, Q.; Feng, Q.; Chen, H. Different flotation performance of ultrafine scheelite under two hydrodynamic cavitation modes. *Minerals* **2018**, *8*, 264. [CrossRef]

107. Tao, D.; Yu, S.; Zhou, X.; Honaker, R.Q.; Parekh, B.K. Picobubble column flotation of fine coal. *Int. J. Coal Prep. Util.* **2008**, *28*, 1–14. [CrossRef]

108. Ma, J.; Hsiao, C.T.; Chahine, G.L. Numerical study of acoustically driven bubble cloud dynamics near a rigid wall. *Ultrason. Sonochemistry* **2018**, *40*, 944–954. [CrossRef] [PubMed]

109. Li, M. Influence of Venturi Tube Geometry and Particle Properties on the Hydrodynamic Cavitation for Fine Particle Flotation. Master's Thesis, University of Alberta, Edmonton, AB, Canada, 2017.

110. Yang, S.; Tsai, P.; Kooij, E.S.; Prosperetti, A.; Zandvliet, H.J.; Lohse, D. Electrolytically generated nanobubbles on highly orientated pyrolytic graphite surfaces. *Langmuir* **2009**, *25*, 1466–1474. [CrossRef] [PubMed]

111. Zhang, L.; Zhang, Y.; Zhang, X.; Li, Z.; Shen, G.; Ye, M.; Fan, C.; Fang, H.; Hu, J. Electrochemically controlled formation and growth of hydrogen nanobubbles. *Langmuir* **2006**, *22*, 8109–8113. [CrossRef] [PubMed]

112. Alheshibri, M.; Jehannin, M.; Coleman, V.A.; Craig, V.S. Does gas supersaturation by a chemical reaction produce bulk nanobubbles? *J. Colloid Interface Sci.* **2019**, *554*, 388–395. [CrossRef]

113. Chen, Q.; Luo, L.; Faraji, H.; Feldberg, S.W.; White, H.S. Electrochemical measurements of single H_2 nanobubble nucleation and stability at Pt nanoelectrodes. *J. Phys. Chem. Lett.* **2014**, *5*, 3539–3544. [CrossRef]

114. Chen, Q.; Wiedenroth, H.S.; German, S.R.; White, H.S. Electrochemical nucleation of stable N_2 nanobubbles at Pt nanoelectrodes. *J. Am. Chem. Soc.* **2015**, *137*, 12064–12069. [CrossRef]

115. Ren, H.; German, S.R.; Edwards, M.A.; Chen, Q.; White, H.S. Electrochemical generation of individual O_2 nanobubbles via H_2O_2 oxidation. *J. Phys. Chem. Lett.* **2017**, *8*, 2450–2454. [CrossRef]

116. Li, M.; Tonggu, L.; Zhan, X.; Mega, T.L.; Wang, L. Cryo-EM visualization of nanobubbles in aqueous solutions. *Langmuir* **2016**, *32*, 11111–11115. [CrossRef]

117. Bui, T.T.; Nguyen, D.C.; Han, M. Average size and zeta potential of nanobubbles in different reagent solutions. *J. Nanoparticle Res.* **2019**, *21*, 173. [CrossRef]

118. Lund, E.J.; LaBelle, J.; Torbert, R.B.; Liou, K.; Peria, W.; Kletzing, C.A.; Kelley, M.C.; Baker, S.D.; Primdahl, F.; Stenbaek-Nielsen, C.; et al. Observation of electromagnetic oxygen cyclotron waves in a flickering aurora. *Geophys. Res. Lett.* **1995**, *22*, 2465–2468. [CrossRef]

119. Leifer, I.; Patro, R.K.; Bowyer, P. A study on the temperature variation of rise velocity for large clean bubbles. *J. Atmos. Ocean. Technol.* **2000**, *17*, 1392–1402. [CrossRef]

120. Vinnett, L.; Sovechles, J.; Gomez, C.; Waters, K. An image analysis approach to determine average bubble sizes using one-dimensional Fourier analysis. *Miner. Eng.* **2018**, *126*, 160–166. [CrossRef]

121. Kim, S.; Kwon, O.; Seo, J.K.; Yoon, J.R. On a nonlinear partial differential equation arising in magnetic resonance electrical impedance tomography. *SIAM J. Math. Anal.* **2002**, *34*, 511–526. [CrossRef]

122. Cho, J.; Perlin, M.; Ceccio, S.L. Measurement of near-wall stratified bubbly flows using electrical impedance. *Meas. Sci. Technol.* **2005**, *16*, 1021. [CrossRef]

123. Manasseh, R.; LaFontaine, R.; Davy, J.; Shepherd, I.; Zhu, Y.G. Passive acoustic bubble sizing in sparged systems. *Exp. Fluids* **2001**, *30*, 672–682. [CrossRef]

124. Spencer, S.J.; Bruniges, R.; Roberts, G.; Sharp, V.; Catanzano, A.; Bruckard, W.J.; Davey, K.J.; Zhang, W. An acoustic technique for measurement of bubble solids mass loading: (b) Monitoring of Jameson cell flotation performance by passive acoustic emissions. *Miner. Eng.* **2012**, *36*, 21–30. [CrossRef]

125. Kracht, W.; Moraga, C. Acoustic measurement of the bubble Sauter mean diameter d_{32}. *Miner. Eng.* **2016**, *98*, 122–126. [CrossRef]

126. Khoshdast, H.; Hassanzadeh, A.; Kowalczuk, P.B.; Farrokhpay, S. Characterization techniques of flotation frothers—A Review. *Miner. Process. Extr. Metall. Rev.* **2022**, 1–25. [CrossRef]

127. Etchepare, R.; Azevedo, A.; Calgaroto, S.; Rubio, J. Removal of ferric hydroxide by flotation with micro and nanobubbles. *Sep. Purif. Technol.* **2017**, *184*, 347–353. [CrossRef]

128. Oh, S.H.; Kim, J.M. Generation and stability of bulk nanobubbles. *Langmuir* **2017**, *33*, 3818–3823. [CrossRef] [PubMed]

129. Ulatowski, K.; Sobieszuk, P.; Mroz, A.; Ciach, T. Stability of nanobubbles generated in water using porous membrane system. *Chem. Eng. Process. Process Intensif.* **2019**, *136*, 62–71. [CrossRef]

130. Qiu, J.; Zou, Z.; Wang, S.; Wang, X.; Wang, L.; Dong, Y.; Zhao, H.; Zhang, L.; Hu, J. Formation and stability of bulk nanobubbles generated by ethanol- water exchange. *Emphysema* **2017**, *18*, 1345–1350. [CrossRef] [PubMed]

131. Fan, F.; Daniel, T.; Honaker, R.; Zhenfu, L. Nanobubble generation and its applications in froth flotation (part IV): Mechanical cells and specially designed column flotation of coal. *Min. Sci. Technol. (China)* **2010**, *20*, 641–671. [CrossRef]

132. Pourkarimi, Z.; Rezai, B.; Noaparast, M.; Nguyen, A.V.; Chehreh Chelgani, S. Proving the existence of nanobubbles produced by hydrodynamic cavitation and their significant effects in powder flotation. *Adv. Powder Technol.* **2021**, *32*, 1810–1818. [CrossRef]

133. Tao, D.; Wu, Z.; Sobhy, A. Investigation of nanobubble enhanced reverse anionic flotation of hematite and associated mechanisms. *Powder Technol.* **2021**, *379*, 12–25. [CrossRef]

134. Ebrahimi, H.; Karamoozian, M.; Saghravani, S.F. Interaction of applying stable micro-nano bubbles and ultrasonic irradiation in coal flotation. *Int. J. Coal Prep. Util.* **2020**, 1–15. [CrossRef]

135. Liu, L.; Hu, S.; Wu, C.; Liu, K.; Weng, L.; Zhou, W. Aggregates characterizations of the ultra-fine coal particles induced by nanobubbles. *Fuel* **2021**, *297*, 120765. [CrossRef]

136. Lei, W.; Zhang, M.; Zhang, Z.; Zhan, N.; Fan, R. Effect of bulk nanobubbles on the entrainment of kaolinite particles in flotation. *Powder Technol.* **2020**, *362*, 84–89. [CrossRef]

137. Olszok, V.; Rivas-Botero, J.; Wollmann, A.; Benker, B.; Weber, A.P. Particle-induced nanobubble generation for material-selective nanoparticle flotation. *Colloids Surf. A Physicochem. Eng. Asp.* **2020**, *592*, 124576. [CrossRef]

138. Calgaroto, S.; Azevedo, A.; Rubio, J. Separation of amine-insoluble species by flotation with nano and microbubbles. *Miner. Eng.* **2016**, *89*, 24–29. [CrossRef]

139. Wu, C.; Wang, L.; Harbottle, D.; Masliyah, J.; Xu, Z. Studying bubble- particle interactions by zeta potential distribution analysis. *J. Colloid Interface Sci.* **2015**, *449*, 399–408. [CrossRef] [PubMed]

140. Hampton, M.A.; Nguyen, A.V. Accumulation of dissolved gases at hydrophobic surfaces in water and sodium chloride solutions: Implications for coal flotation. *Miner. Eng.* **2009**, *22*, 786–792. [CrossRef]

141. Vaziri Hassas, B.; Jin, J.; Dang, L.X.; Wang, X.; Miller, J.D. Attachment, coalescence, and spreading of carbon dioxide nanobubbles at pyrite surfaces. *Langmuir* **2018**, *34*, 14317–14327. [CrossRef] [PubMed]

142. Deng, X.; Lv, B.; Cheng, G.; Lu, Y. Mechanism of micro/nano-bubble formation and cavitation effect on bubbles size distribution in flotation. *Physicochem. Probl. Miner. Process.* **2020**, *56*, 504–512. [CrossRef]

143. Li, H.; Afacan, A.; Liu, Q.; Xu, Z. Study interactions between fine particles and micron size bubbles generated by hydrodynamic cavitation. *Miner. Eng.* **2015**, *84*, 106–115. [CrossRef]

144. Xing, Y.; Gui, X.; Cao, Y.; Wang, D.; Zhang, H. Clean low-rank-coal purification technique combining cyclonic- static microbubble flotation column with collector emulsification. *J. Clean. Prod.* **2017**, *153*, 657–672. [CrossRef]

145. Rulyov, N.N.; Filippov, L.O.; Kravchenko, O.V. Combined microflotation of glass beads. *Colloids Surf. A Physicochem. Eng. Asp.* **2020**, *598*, 124810. [CrossRef]

146. Rulyov, N.N.; Sadovskiy, D.Y.; Rulyova, N.A.; Filippov, L.O. Column flotation of fine glass beads enhanced by their prior heteroaggregation with microbubbles. *Colloids Surf. A Physicochem. Eng. Asp.* **2021**, *617*, 126398. [CrossRef]

147. Zhou, Z.A.; Chow, R.S.; Cleyle, P.; Xu, Z.H.; Masliyah, J.H. Effect of dynamic bubble nucleation on bitumen flotation. *Can. Metall. Q.* **2010**, *49*, 363–372. [CrossRef]

148. Ross, V.; Singh, A.; Pillay, K. Improved flotation of PGM tailings with a high-shear hydrodynamic cavitation device. *Miner. Eng.* **2019**, *137*, 133–139. [CrossRef]

149. Li, C.; Xu, M.; Zhang, H. The interactions between coal particles with different hydrophobicity and bulk nanobubbles in natural water. *Int. J. Coal Prep. Util.* **2019**, *42*, 463–474. [CrossRef]

150. Zhang, Z.; Ren, L.; Zhang, Y. Role of nanobubbles in the flotation of fine rutile particles. *Miner. Eng.* **2021**, *172*, 107140. [CrossRef]

151. Zhou, J.Z.; Li, H.; Chow, R.S.; Liu, Q.; Xu, Z.; Masliyah, J. Role of mineral flotation technology in improving bitumen extraction from mined Athabasca oil sands- II. Flotation hydrodynamics of water-based oil sand extraction. *Can. J. Chem. Eng.* **2020**, *98*, 330–352. [CrossRef]

152. Xu, G.; Chen, Y.; Bu, X.; Dong, X.; Xie, G.; Sun, Y. Separation performance of mechanical flotation cell and cyclonic microbubble flotation column: In terms of the beneficiation of high-ash coal fines. *Energy Sources Part A Recovery Util. Environ. Eff.* **2020**, *42*, 2845–2855. [CrossRef]

153. Chipakwe, V.; Jolstera, R.; Chelgani, S.C. Nanobubble-Assisted Flotation of Apatite Tailings: Insights on Beneficiation Options. *ACS Omega* **2021**, *6*, 13888–13894. [CrossRef]

154. Chipakwe, V.; Sand, A.; Chelgani, S.C. Nanobubble assisted flotation separation of complex Pb–Cu–Zn sulfide ore—Assessment of process readiness. *Sep. Sci. Technol.* **2021**, *57*, 1351–1358. [CrossRef]

155. Lee Black, D.; McQuay, M.Q.; Bonin, M.P. Laser-based techniques for particle-size measurement: A review of sizing methods and their industrial applications. *Prog. Energy Combust. Sci.* **1996**, *22*, 267–306. [CrossRef]

156. Grubbs, J.; Tsaknopoulos, K.; Massar, C.; Young, B.; O'Connell, A.; Walde, C.; Birt, A.; Siopis, M.; Cote, D. Comparison of laser diffraction and image analysis techniques for particle size-shape characterization in additive manufacturing applications. *Powder Technol.* **2021**, *391*, 20–33. [CrossRef]

157. Yan-ge, H. Rectification study of particle analysing result between laser instrument and sieving method. *Mathematics* **2012**, *30*, 716–723.

158. Zhang, S.Y.; Lv, F.Y.; Xia, Z.M.; Li, N.; Wu, M. The feasibility study of laser particle size analyzer for thick pastes. *Appl. Mech. Mater.* **2013**, *372*, 428–432. [CrossRef]

159. Ilic, M.; Budak, I.; Vucinic Vasic, M.; Nagode, A.; Kozmidis-Luburić, U.; Hodolic, J.; Puskar, T. Size and shape particle analysis by applying image analysis and laser diffraction—Inhalable dust in a dental laboratory. *Measurement* **2015**, *66*, 109–117. [CrossRef]

160. Hou, J.; Ci, H.; Wang, P.; Wang, C.; Lv, B.; Miao, L.; You, G. Nanoparticle tracking analysis versus dynamic light scattering: Case study on the effect of Ca^{2+} and alginate on the aggregation of cerium oxide nanoparticles. *J. Hazard. Mater.* **2018**, *360*, 319–328. [CrossRef] [PubMed]

161. Qian, H.; Sheetz, M.P.; Elson, E.L. Single particle tracking. Analysis of diffusion and flow in two-dimensional systems. *Biophys. J.* **1991**, *60*, 910–921. [CrossRef]

162. Filipe, V.; Hawe, A.; Jiskoot, W. Critical evaluation of nanoparticle tracking analysis (NTA) by nanosight for the measurement of nanoparticles and protein aggregates. *Pharm. Res.* **2010**, *27*, 796–810. [CrossRef]

163. Mehrabi, K.; Nowack, B.; Arroyo Rojas Dasilva, Y.; Mitrano, D.M. Improvements in nanoparticle tracking analysis to measure particle aggregation and mass distribution: A case study on engineered nanomaterial stability in incineration landfill leachates. *Environ. Sci. Technol.* **2017**, *51*, 5611–5621. [CrossRef]

164. Babick, F. Dynamic light scattering (DLS). In *Characterization of Nanoparticles*; Elsevier: Amsterdam, The Netherlands, 2020; Chapter 3.2.1; pp. 137–172.

165. Jin, J.; Wang, R.; Tang, J.; Yang, L.; Feng, Z.; Xu, C.; Yang, F.; Gu, N. Dynamic tracking of bulk nanobubbles from microbubbles shrinkage to collapse. *Colloids Surf. A Physicochem. Eng. Asp.* **2020**, *589*, 124430. [CrossRef]
166. Sartor, M. Dynamic Light Scattering to Determine the Radius of Small Beads in Brownian Motion in a Solution. Course Material. University of California: San Diego, CA, USA, 2014. Available online: https://neurophysics.ucsd.edu/courses/physics_173_273/dynamic_light_scattering_03.pdf (accessed on 10 January 2022).
167. Aljamali, N. Zetasizer technique in biochemistry. *Biochem. Anal. Biochem.* **2015**, *4*, 2.
168. Sjogreen, C.; Tellez, D.A.; Perez, J.E.R.; Hurtado, P.C.P.; Roa-Rojas, J. Experimental study of nanobubbles in salt solutions. *Rev. Acad. Colomb. Cienc. Ex. Fis. Nat.* **2018**, *42*, 41–48. [CrossRef]
169. Seo, Y.; Jhe, W. Atomic force microscopy and spectroscopy. *Rep. Prog. Phys.* **2007**, *71*, 016101. [CrossRef]
170. Rabinowitz, J.; Whittier, E.; Liu, Z.; Jayant, K.; Frank, J.; Shepard, K. Nanobubble-controlled nanofluidic transport. *Sci. Adv.* **2020**, *6*, eabd0126. [CrossRef] [PubMed]
171. Zhou, L.; Wang, S.; Zhang, L.; Hu, J. Generation and stability of bulk nanobubbles: A review and perspective. *Curr. Opin. Colloid Interface Sci.* **2021**, *53*, 101439. [CrossRef]
172. Wesley, D.J.; Toolan, D.T.; Brittle, S.A.; Howse, J.R.; Zimmerman, W.B. Development of an optical microscopy system for automated bubble cloud analysis. *Appl. Opt.* **2016**, *55*, 6102–6107. [CrossRef] [PubMed]
173. Karpitschka, S.; Dietrich, E.; Seddon, J.R.; Zandvliet, H.J.; Lohse, D.; Riegler, H. Nonintrusive optical visualization of surface nanobubbles. *Phys. Rev. Lett.* **2012**, *109*, 066102. [CrossRef]
174. Chan, C.U.; Ohl, C.D. Total internal reflection fluorescence microscopy for the study of nanobubble dynamics. *Phys. Rev. Lett.* **2012**, *109*, 174501. [CrossRef]
175. Drzymala, J.; Kowalczuk, P.B. Classification of flotation frothers. *Minerals* **2018**, *8*, 53. [CrossRef]
176. Park, H.; Ng, C.Y.; Wang, L. Bubble size in a flotation column with oscillatory air supply in the presence of frothers. *Miner. Process. Extr. Metall. Rev.* **2021**, 1–9. [CrossRef]
177. Urbina, R.H. Recent developments and advances in formulations and applications of chemical reagents used in froth flotation. *Miner. Process. Extr. Metall. Rev.* **2003**, *24*, 139–182. [CrossRef]
178. Moreno, Y.S.; Bournival, G.; Ata, S. Classification of flotation frothers—A statistical approach. *Chem. Eng. Sci.* **2022**, *248*, 117252. [CrossRef]
179. Calgaroto, S.; Wilberg, K.Q.; Rubio, J. On the nanobubbles interfacial properties and future applications in flotation. *Miner. Eng.* **2014**, *60*, 33–40. [CrossRef]
180. Jia, W.; Ren, S.; Hu, B. Effect of water chemistry on zeta potential of air bubbles. *Int. J. Electrochem. Sci.* **2013**, *8*, 5828–5837.
181. Phan, K.; Truong, T.; Wang, Y.; Bhandari, B. Effect of electrolytes and surfactants on generation and longevity of carbon dioxide nanobubbles. *Food Chem.* **2021**, *363*, 130299. [CrossRef] [PubMed]
182. Nazari, S.; Shafaei, S.Z.; Gharabaghi, M.; Ahmadi, R.; Shahbazi, B.; Tehranchi, A. New approach to quartz coarse particles flotation using nanobubbles, with emphasis on the bubble size distribution. *Int. J. Nanosci.* **2020**, *19*, 1850048. [CrossRef]
183. Laskowski, J.S. Testing flotation frothers. *Physicochem. Probl. Miner. Process.* **2004**, *38*, 13–22.
184. Laskowski, J.S. Frothers and Flotation Froth. *Miner. Process. Extr. Metall. Rev.* **1993**, *12*, 61–89. [CrossRef]
185. Khoshdast, H.; Sam, A. Flotation frothers: Review of their classifications, properties and preparation. *Open Miner. Process. J.* **2011**, *4*, 25–44. [CrossRef]
186. Aveyard, R.; Binks, B.; Fletcher, P.; Peck, T.; Rutherford, C. Aspects of aqueous foam stability in the presence of hydrocarbon oils and solid particles. *Adv. Colloid Interface Sci.* **1994**, *48*, 93–120. [CrossRef]
187. Yoon, R.H.; Luttrell, G.H. The effect of bubble size on fine particle flotation. *Miner. Process. Extr. Metall. Rev.* **1989**, *5*, 101–122. [CrossRef]
188. Farrokhpay, S.; Filippov, L.; Fornasiero, D. Flotation of fine particles: A review. *Miner. Process. Extr. Metall. Rev.* **2021**, *42*, 473–483. [CrossRef]
189. Cho, Y.S.; Laskowski, J.S. Bubble coalescence and its effect on dynamic foam stability. *Can. J. Chem. Eng.* **2002**, *80*, 299–305. [CrossRef]
190. Khoshdast, H.; Abbasi, H.; Sam, A.; Noghabi, K.A. Frothability and surface behavior of a rhamnolipid biosurfactant produced by Pseudomonas aeruginosa MA01. *Biochem. Eng. J.* **2012**, *60*, 127–134. [CrossRef]
191. Zhang, X.H.; Khan, A.; Ducker, W.A. A nanoscale gas state. *Phys. Rev. Lett.* **2007**, *98*, 136101. [CrossRef] [PubMed]
192. Switkes, M.; Ruberti, J. Rapid cryofixation/freeze fracture for the study of nanobubbles at solid-liquid interfaces. *Appl. Phys. Lett.* **2004**, *84*, 4759–4761. [CrossRef]
193. Steitz, R.; Gutberlet, T.; Hauss, T.; Klösgen, B.; Krastev, R.; Schemmel, S.; Simonsen, A.C.; Findenegg, G.H. Nanobubbles and their precursor layer at the interface of water against a hydrophobic substrate. *Langmuir* **2003**, *19*, 2409–2418. [CrossRef]
194. Johnson, B.D.; Cooke, R.C. Generation of stabilized microbubbles in seawater. *Science* **1981**, *213*, 209–211. [CrossRef]
195. Jeldres, R.I.; Forbes, L.; Cisternas, L.A. Effect of seawater on sulfide ore flotation: A review. *Miner. Process. Extr. Metall. Rev.* **2016**, *37*, 369–384. [CrossRef]
196. Bournival, G.; Zhang, F.; Ata, S. Coal flotation in saline water: Effects of electrolytes on interfaces and industrial practice. *Miner. Process. Extr. Metall. Rev.* **2021**, *42*, 53–73. [CrossRef]
197. Hewage, S.A.; Kewalramani, J.; Meegoda, J.N. Stability of nanobubbles in different salts solutions. *Colloids Surf. A Physicochem. Eng. Asp.* **2021**, *609*, 125669. [CrossRef]

198. Uchida, T.; Liu, S.; Enari, M.; Oshita, S.; Yamazaki, K.; Gohara, K. Effect of NaCl on the lifetime of micro-and nanobubbles. *Nanomaterials* **2016**, *6*, 31. [CrossRef]

199. Basarova, P.; Zawala, J.; Zednikova, M. Interactions between a small bubble and a greater solid particle during the flotation process. *Miner. Process. Extr. Metall. Rev.* **2019**, *40*, 410–426. [CrossRef]

200. Fan, M.; Zhao, Y.; Tao, D. Fundamental Studies of Nanobubble Generation and Applications in Flotation. In *Separation Technologies for Minerals, Coal, and Earth Resources*; Society for Mining, Metallurgy, and Exploration: Englewood, CO, USA, 2012; pp. 457–469.

201. Farrokhpay, S.; Filippova, I.; Filippov, L.; Picarra, A.; Rulyov, N.; Fornasiero, D. Flotation of fine particles in the presence of combined microbubbles and conventional bubbles. *Miner. Eng.* **2020**, *155*, 106439. [CrossRef]

202. Fan, M.; Tao, D. A study on picobubble enhanced coarse phosphate froth flotation. *Sep. Sci. Technol.* **2008**, *43*, 1–10. [CrossRef]

203. Li, G.; Cao, Y.; Liu, J.; Wang, D. Cyclonic flotation column of siliceous phosphate ore. *Int. J. Miner. Process.* **2012**, *110–111*, 6–11. [CrossRef]

204. Johansson, G.; Pugh, R. The influence of particle size and hydrophobicity on the stability of mineralized froths. *Int. J. Miner. Process.* **1992**, *34*, 1–21. [CrossRef]

205. Kennedy, D.L. Redesign of Industrial Column Flotation Circuits Based on a Simple Residence Time Distribution Model. Master's Thesis, Virginia Tech., Blacksburg, VA, USA, 2008.